

1 **EPIDURAL ELECTRICAL STIMULATION OF THE CERVICAL DORSAL ROOTS RESTORES**  
2 **VOLUNTARY UPPER LIMB CONTROL IN PARALYZED MONKEYS**

3 B. Barra<sup>1,2,\*</sup>, S. Conti<sup>1,\*</sup>, M.G. Perich<sup>3</sup>, K. Zhuang<sup>1</sup>, G. Schiavone<sup>4</sup>, F. Fallegger<sup>4</sup>, K. Galan<sup>5,7</sup>, N.  
4 D. James<sup>5</sup>, Q. Barraud<sup>5,7</sup>, M. Delacombaz<sup>1,7</sup>, M. Kaeser<sup>1</sup>, E. M. Rouiller<sup>1</sup>, T. Milekovic<sup>3,7</sup>, S.  
5 Lacour<sup>4</sup>, J. Bloch<sup>6,7</sup>, G. Courtine<sup>5,6,7</sup> and M. Capogrosso<sup>1,2,8</sup>

6 <sup>1</sup> Platform of Translational Neuroscience, Department of Neuroscience and Movement Sciences, Faculty of Sciences and Medicine,  
7 University of Fribourg, Fribourg, Switzerland

8 <sup>2</sup> Rehab and Neural Engineering Labs, University of Pittsburgh, Pittsburgh, USA.

9 <sup>3</sup> Department of Fundamental Neuroscience, Faculty of Medicine, University of Geneva, Geneva, Switzerland

10 <sup>4</sup> Bertarelli Foundation Chair in Neuroprosthetic Technology, Laboratory for Soft Bioelectronic Interfaces, Institute of  
11 Microengineering, Institute of Bioengineering, Centre for Neuroprosthetics, École Polytechnique Fédérale de Lausanne, Geneva,  
12 Switzerland.

13 <sup>5</sup> Center for Neuroprosthetics and Brain Mind Institute, School of Life Sciences, Ecole Polytechnique Fédérale de Lausanne,  
14 Lausanne, Switzerland.

15 <sup>6</sup> Department of Neurosurgery, CHUV, Lausanne, Switzerland;

16 <sup>7</sup> Defitech Center for Interventional Neurotherapies (NeuroRestore), University Hospital Lausanne (CHUV), University of Lausanne  
17 (UNIL) and Ecole Polytechnique Fédérale de Lausanne, Lausanne, Switzerland.

18 <sup>8</sup> Department of Neurological Surgery, University of Pittsburgh, Pittsburgh, USA

19 \*these authors contributed equally to this work

20 Correspondence to: Marco Capogrosso - [mcapo@pitt.edu](mailto:mcapo@pitt.edu)

21

22

23

24 **SUMMARY**

25 Recovering arm control is a top priority for people with paralysis. Unfortunately, the complexity of  
26 the neural mechanisms underlying arm control practically limited the effectiveness of  
27 neurotechnology approaches. Here, we exploited the neural function of surviving spinal circuits  
28 to restore voluntary arm and hand control in three monkeys with spinal cord injury using spinal  
29 cord stimulation. Our neural interface leverages the functional organization of the dorsal roots to  
30 convey artificial excitation via electrical stimulation to relevant spinal segments at appropriate  
31 movement phases. Stimulation bursts targeting specific spinal segments produced sustained arm  
32 movements enabling monkeys with arm paralysis to perform an unconstrained reach-and-grasp  
33 task. Stimulation specifically improved strength, task performances and movement quality.  
34 Electrophysiology suggested that residual descending inputs were necessary to produce  
35 coordinated movements. The efficacy and reliability of our approach hold realistic promises of  
36 clinical translation.

37

## 38 INTRODUCTION

39 More than 5 million people in the US currently live with some form of motor paralysis<sup>1</sup>. Stroke and  
40 spinal cord injury (SCI) are the main causes with hundreds of thousands of new cases per year<sup>2</sup>.  
41 Impairments of the hand and arm are particularly problematic, representing a major unmet need  
42 for both SCI and stroke patient populations<sup>3,4</sup>. Indeed, even mild deficits in hand function lead to  
43 significant degradation of quality of life. Unfortunately, recovery of hand and arm motor function  
44 is still an unsolved clinical challenge.

45  
46 Generated in the cerebral cortex, upper limb motor commands are relayed to subcortical and  
47 spinal circuits that activate motoneurons and regulate sensory inputs to produce skilled motor  
48 actions<sup>5-8</sup>. Spinal cord injury (SCI), or stroke, damage these communication pathways generating  
49 impairments in sensory regulation and motor functions that lead to motor paralysis.

50 Historically, neurotechnologies were conceived around the idea of restoring movements in  
51 paralyzed subjects via a technological bypass. Such solution would use signals from cortical  
52 areas as inputs and artificially compensate for lack of motoneuron activation by producing desired  
53 muscle activity below the lesion<sup>9</sup>. For example, functional electrical stimulation (FES) was used  
54 to activate arm muscles in response to intracortical neural activity from the motor cortex<sup>10,11</sup>. This  
55 pioneering concept allowed paralyzed monkeys and humans to perform voluntary grasping  
56 tasks<sup>10-13</sup>. However, translation of these concepts into daily clinical practice is hindered by two  
57 distinct limitations. First, the artificial motoneuron recruitment order generated by FES induces  
58 muscle fatigue<sup>14</sup> which is particularly problematic for arm movements. Indeed, fatigue prevents  
59 the generation of sustained forces and consequently FES fails to enable sustained three-  
60 dimensional arm movements that are required for daily activities. Second, since FES bypasses  
61 surviving circuits in the spinal cord, complex stimulation protocols<sup>15</sup> and sophisticated decoding  
62 algorithms<sup>10,13</sup> are required to orchestrate the activation of multiple muscles and produce  
63 functional movements. As a result, these systems require an articulated combination of hardware  
64 and software. Unfortunately, this complexity does not cope well with dynamic clinical  
65 environments that need robust and practical solutions for a rapid set up and large-scale use.

66  
67 In contrast, epidural electrical stimulation (EES) of the lumbar spinal cord exploits surviving spinal  
68 circuits and supra-spinal connections after injury to produce movements<sup>16</sup>. Similar to intraspinal  
69 stimulation<sup>17-19</sup>, EES engages motoneurons via direct recruitment of large sensory afferents<sup>20,21</sup>  
70 leading to widespread excitatory post-synaptic potentials in the spinal cord. More importantly,  
71 since motoneurons are recruited via natural synaptic inputs, EES generates a natural recruitment  
72 order<sup>22,23</sup> that is resistant to artificial fatigue. This enables the production of forces that can sustain  
73 the whole-body weight<sup>24</sup>. Moreover, engagement of motoneurons from pre-synaptic pathways  
74 allows residual descending inputs and spinal circuits to control motoneurons excitability and  
75 produce voluntary movement after complete motor paralysis<sup>25,26</sup>.

76  
77 Building on animal models<sup>27-29</sup>, recent clinical studies have shown that continuous stimulation  
78 delivered through epidural implants on the dorsal aspect of the lumbosacral spinal cord increased  
79 muscle strength, voluntary muscle activation and single joint movements in people with complete  
80 leg paralysis<sup>26,30,31</sup>. More strikingly, when coupled with targeted physical rehabilitation protocols,  
81 continuous EES restored weight bearing locomotion in subjects with severe SCI<sup>32,33</sup>. These  
82 outstanding clinical results prompted experimental studies aiming at verifying whether EES could  
83 be used to promote also upper limb movements after SCI<sup>34</sup>. Unfortunately, while clinical studies  
84 showed some success in improving hand grip force with both epidural and non-invasive  
85 approaches<sup>35,36</sup>, continuous EES did not produce results of similar outstanding efficacy as those

86 observed for the lower limbs<sup>32,33</sup>. In fact, clinical outcomes were similar to those obtained with  
87 surface FES<sup>37</sup>.

88 Reasons for this discrepancy may stem from the complexity of upper limb motor control and  
89 biomechanics compared to locomotion. Indeed, in contrast to pattern-driven<sup>38,39</sup> and repetitive  
90 locomotor movements, upper limb movements are composed by a non-repetitive and task-  
91 dependent combination of movement modules which are highly dependent from sophisticated  
92 cortico-spinal control<sup>7,40–44</sup> and accurate sensory feedback<sup>42,45–47</sup>. Because of this intrinsic  
93 complexity, non-specific neuromodulation could limit the efficacy of EES by exciting all spinal  
94 segments simultaneously, irrespectively of movement phase. More importantly, unspecific and  
95 continuous stimulation of the sensory afferents through EES disrupts natural sensory inputs<sup>23</sup>  
96 thus hindering spinal regulation of movements which is critical in dexterous upper limb control<sup>45–  
97 47</sup>.

98 We and others have shown that it is possible to direct electrical stimulation of the spinal cord to  
99 target restricted segments during appropriate times<sup>17,48,49</sup>. These spatio-temporal stimulation  
100 protocols enabled voluntary locomotion in monkeys with SCI as early as day 6 post injury without  
101 any physical training<sup>50</sup> and within 2 weeks post implantation in humans with complete leg  
102 paralysis<sup>51</sup>. This approach exploits the somato-topography of the spinal sensory system to  
103 selectively engage restricted spinal regions<sup>21,49</sup>. Unfortunately, non-invasive technologies and  
104 clinically approved electrodes are unfit for this scope<sup>52,53</sup> because of their limits in selectivity.  
105 Therefore, we hypothesized that a neural interface, specifically designed to target the cervical  
106 dorsal roots, could enable the administration of spatio-temporal stimulation patterns to the cervical  
107 spinal cord. We tested this hypothesis in three monkeys with a unilateral cervical SCI. We  
108 designed a personalized epidural interface to target primary afferents within the cervical dorsal  
109 roots. We hypothesized that the electrical stimulation of the roots with bursts linked to movement  
110 attempts would enable voluntary motor control and improve functional deficits of the arm and hand  
111 that emerge after SCI. Specifically we tested for improvements in muscle strength, dexterity and  
112 ability to execute three-dimensional functional tasks in full independence. Finally, we verified that  
113 the mechanisms enabling the voluntary recruitment of motoneurons in the cervical spinal cord  
114 were similar to those occurring during EES of the lumbosacral circuits.

115

## 116 **Results**

117

### 118 **Natural arm movements**

119 Clinically effective systems should enable truly functional arm movements rather than simplified  
120 tasks such as single-joint movements. A functional arm movement entails a coordinated activation  
121 of arm muscles to achieve a desired movement while supporting the arm weight at all times. Most  
122 of daily activities require arm extension (reach) and flexion (pull), combined with a hand-grasp  
123 without a constrained timing or structure. Consequently, we developed a robotic platform allowing  
124 the quantification of reach, grasp and pull movements<sup>54</sup> that would feel natural and unconstrained  
125 to monkeys both in trajectory and timings (**Figure 1A**). We trained three adult *Macaca fascicularis*  
126 monkeys to reach for, grasp, and pull an instrumented object placed on the end effector of our  
127 robotic arm (**Figure 1B**). Movement trajectories were not constrained neither kinematically nor in  
128 time. Monkeys waited for the go signal, reached for the object and pulled to receive a food or juice  
129 reward when the object crossed a pre-defined displacement threshold<sup>54</sup>. Monkeys intuitively and  
130 rapidly<sup>29,30</sup> learned this task by developing their own individual kinematic strategies (**Extended  
131 Data Figure 1**) and personal movement speeds. We then designed a battery of electrophysiology  
132 and kinematic measurements to evaluate functional outcomes on task performances, muscle

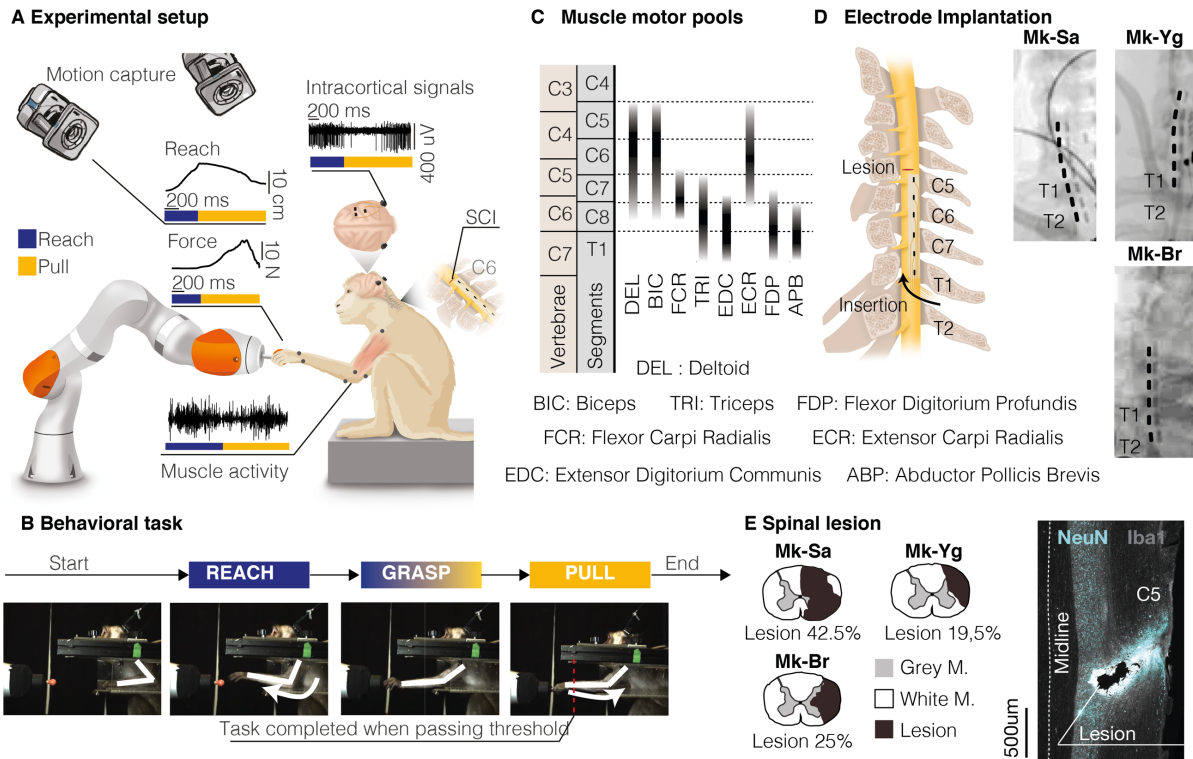


**Figure 1. Experimental framework. (A)** Schematic of the behavioral experimental platform. While the animals were performing a robotic reach, grasp and pull task, we measured 3D forces applied to the robot joints, full-limb kinematics, electromyographic (EMG) activity from eight muscles of the arm and hand, and intra-cortical signals from sensorimotor areas. **(B)** Schematic illustration of the task. Monkeys were trained to reach for, grasp, and pull a target object placed at the end effector of a robotic arm. We considered a movement complete when a target spatial threshold was crossed during pull. **(C)** Motoneurons pool distribution of arm and hand muscles in the cervical spinal cord in relation to vertebrae and spinal segments (adapted from Jenny and Inukai, 1983). Deltoid (DEL), Biceps Brachii (BIC), Flexor Carpi Radialis (FCR), Triceps Brachii (TRI), Extensor Digitorum Communis (EDC), Extensor Carpi Radialis (ECR), Flexor Digitorum Profundus (FDP), Abductor Pollicis Brevis (APB). **(D)** Schematic representation of spinal implant positioning and X-ray scans of the epidural implant in the three monkeys (Mk-Sa, Mk-Br and Mk-Yg). **(E)** Anatomical reconstruction of the cervical spinal cord lesion (black area) for the 3 monkeys, shown on a transversal section (the percentage indicates the portion of the total spinal cord area that was injured on this transversal plane). On the right, representative image of longitudinal section of the spinal cord of Mk-Br around the lesion site stained with NeuN (neuronal cell bodies) and Iba1 (microglia). Copyright Jemère Ruby.

133 activation, muscle strength and movement dexterity. Specifically, we quantified full-limb 3D  
 134 kinematics (Vicon Motion Systems, Oxford, UK), pulling forces, and electromyographic (EMG)  
 135 signals from intramuscular leads in eight arm muscles (**Figure 1A, Extended Data Figure 1**).  
 136 Before SCI, we observed clear bursts of EMG activity from all hand and arm muscles during the  
 137 three movement phases: reach, grasp, and pull in all monkeys. Finally, to document the  
 138 involvement of cortical neurons during movement enabled by EES and to extract signals that  
 139 could also be used to link stimulation bursts to movement phase onset, we implanted multi-  
 140 microelectrode arrays (Blackrock Microsystems, Salt Lake City, USA) in the arm/hand region of  
 141 the right sensorimotor (M1, S1) and ventral premotor (PMv) cortex. We validated these recordings  
 142 by verifying that neural activity was consistently modulated with kinematics pre-injury and with the  
 143 three movement phases as largely expected<sup>54</sup> (**Figure 1, Extended Data Figure 1**). In summary,

144 we analyzed natural arm movements in monkeys and concluded that in order for stimulation  
145 protocols to be effective, it was important to support reach, grasp and pull independently with  
146 specific parameters for each animal.

147  
148

### 149 **Personalized spinal interface**

150 To design an optimal interface, we studied the anatomy of the monkey cervical spinal cord. We  
151 extrapolated available anatomical information from literature and found that, similar to humans,  
152 motoneurons innervating arm muscles in the monkeys are segmentally organized<sup>55</sup> (**Figure 1C**).  
153 We previously showed that stimulation of a single cervical dorsal root will recruit motoneurons  
154 that receive direct afferent inputs from that root<sup>53</sup>. Exploiting this property allows to obtain a  
155 segmental recruitment order of motoneurons that can be targeted to promote specific movement  
156 phases<sup>49,51,56</sup>. Therefore, we designed a spinal interface that could target each root independently.  
157 We achieved this by placing contacts on the lateral aspect of the cord to target the entry zone of  
158 each individual root<sup>53</sup>. Since each monkey displayed a unique anatomy, we tailored the design of  
159 our interface to each specific subject. For this, we measured white matter diameter and vertebral  
160 canal features from computed tomography (CT) and magnetic resonance imaging (MRI). We then  
161 spaced the electrodes rostro-caudally and medio-laterally to match the transversal and  
162 longitudinal dimensions of the cord of each animal (**Extended Data Figure 2A, 2B**). This allowed  
163 us to simplify the neural interface architecture by minimizing the number of contacts while  
164 maintaining high muscle recruitment specificity<sup>57</sup>. We then designed a surgical strategy to position  
165 the epidural interface between the C6 and T1 dorsal roots (**Figure 1D**). We performed  
166 laminectomies between the T1 and T2 vertebrae and the C5 and C6 vertebrae, then pulled the  
167 neural interface through the intermediate epidural space with the help of a custom soft inserter<sup>57</sup>.

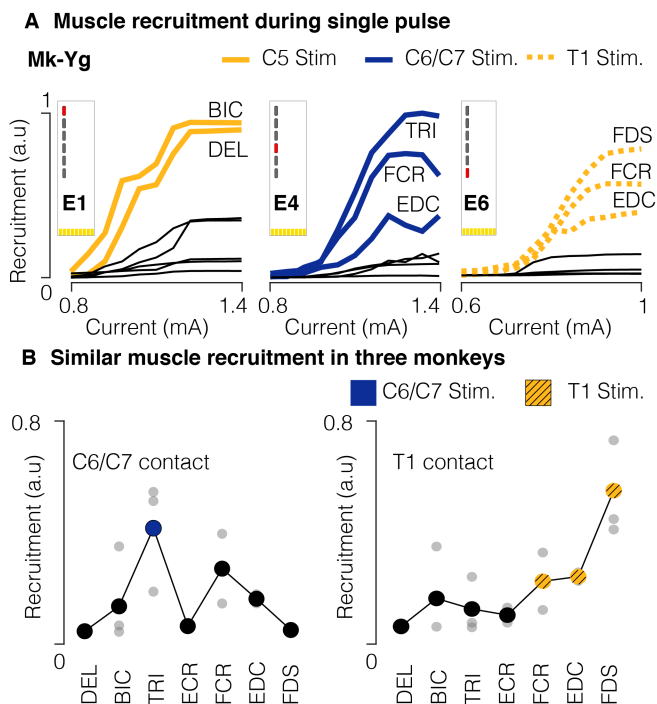


**Figure 2. Muscle recruitment of spinal stimulation. (A)** Examples of muscle recruitment obtained by stimulating (1 Hz) at C5, C6/C7, and T1 spinal segments (Mk-Yg). **(B)** Average muscle activations elicited from C6/C7 and T1 contacts in n=3 monkeys (grey bullets: for each animal, average recruitment across all stimulation currents. Big bullets: mean of average recruitments across animals).

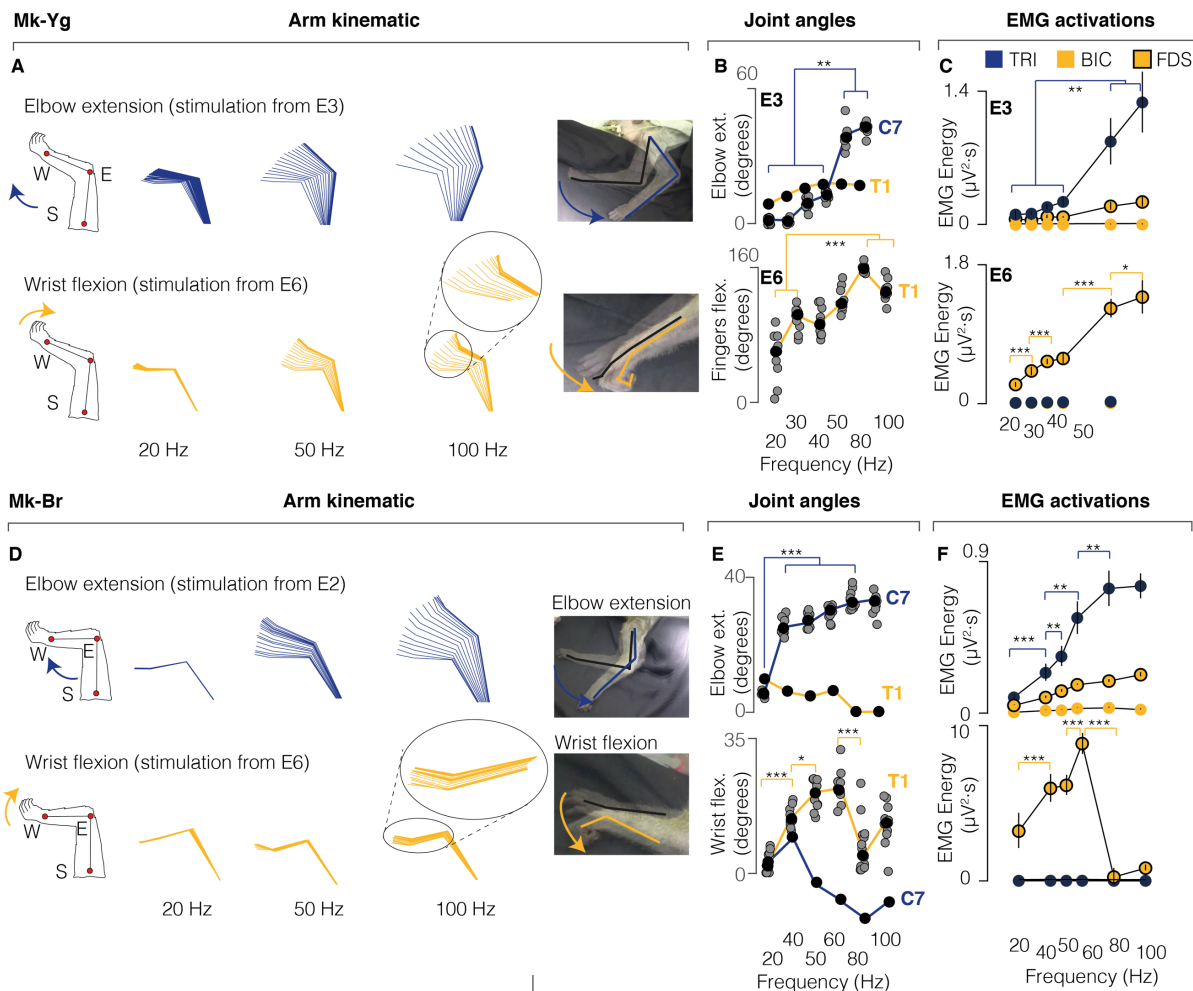


**Figure 3. EES produces functional joint movements in anesthetized animals. (A)** Stick diagram schematic of elbow extension and wrist flexion movements elicited by pulse-trains of stimulation in anesthetized conditions in Mk-Yg. **(B)** Modulation of maximal joint angles achieved by pulse-trains of stimulation at different frequencies, in anesthetized conditions in Mk-Yg. Stimulation was delivered at C7 (blue) and T1 (yellow). Statistics performed with Wilcoxon Ranksum test and Bonferroni correction. Asterisks: \* $p < 0.05$ , \*\* $p < 0.01$ , \*\*\* $p < 0.001$  **(C)** Triceps (blue), biceps (yellow), and flexor digitorum superficialis (yellow with black border) activity elicited by pulse-trains of stimulation at different frequencies, in anesthetized conditions in Mk-Yg. Bullets represent mean values and bars are standard deviation. Statistics performed with Wilcoxon Ranksum test and Bonferroni correction. Asterisks: \* $p < 0.05$ , \*\* $p < 0.01$ , \*\*\* $p < 0.001$  **(D)** Stick diagram schematic of elbow extension and wrist flexion movements elicited by pulse-trains of stimulation in anesthetized conditions in Mk-Br. Statistics performed with Wilcoxon Ranksum test and Bonferroni correction. Asterisks: \* $p < 0.05$ , \*\* $p < 0.01$ , \*\*\* $p < 0.001$  **(E)** Modulation of maximal joint angles achieved by pulse-trains of stimulation at different frequencies, in anesthetized conditions in Mk-Br. Stimulation was delivered at C7 (blue) and T1 (yellow) **(F)** Triceps (blue), biceps (yellow), and flexor digitorum superficialis (yellow with black border) activity elicited by pulse-trains of stimulation at different frequencies, in anesthetized conditions in Mk-Br. Bullets represent mean values and bars are standard deviation. Statistics performed with Wilcoxon Ranksum test and Bonferroni correction. Asterisks: \* $p < 0.05$ , \*\* $p < 0.01$ , \*\*\* $p < 0.001$

168 We verified that the position of the array remained stable for the entire duration of the study (up  
 169 to 3 weeks) through repeated X-ray imaging (**Figure 1D**, **Extended Data Figure 2C**). During the  
 170 same surgery, we performed a unilateral spinal cord injury at the C5/C6 segments (**Figure 1E**)

171 aiming at transecting the cortico-spinal tract that is located on the lateral aspect of the white matter  
172 in monkeys. This type of lesion is amply described in literature and induces unilateral arm and  
173 hand paralysis<sup>58,59</sup> while preserving important bodily functions such as bladder control.  
174 Postmortem immunohistochemistry analysis of the spinal cords showed that the spinal interface  
175 did not damage the cervical cord in any of the three monkeys but did reveal that Mk-Br received  
176 an unplanned compression injury at the insertion site (T3 spinal segment). Given the caudal  
177 position of this contusion it is likely for it to have occurred during implantation (**Extended Data**  
178 **Figure 2D**). Since the T3 segment is below the innervation of the arm motoneurons, this lesion  
179 did not affect the phenotype of arm and hand motor deficits which did not differ from the other  
180 monkeys (see Methods).

181 In summary, we designed a spinal interface to selectively recruit the cervical dorsal roots. We  
182 tailored the interface to the specific anatomy of each monkey and designed a surgical strategy to  
183 perform a consistent and stable implantation.

184

### 185 **Cervical EES produces functional joint movements and grasp in anaesthetized monkeys**

186 We next assessed the selectivity of the epidural interface. In propofol anaesthetized monkeys, we  
187 delivered asymmetric, charge-balanced biphasic pulses of EES at low repetition rate (1Hz) at  
188 various current amplitudes from each contact. Minimum and maximum amplitude values were  
189 selected as the first subthreshold and first saturation current value respectively. As predicted<sup>53</sup>,  
190 different stimulation contacts generated muscle recruitment patterns that mirrored the segmental  
191 organization of cervical motoneurons (**Figure 2A, Extended Data Figure 3**). Specifically,  
192 contacts located at C8/T1 level (caudal) elicited spinal reflexes mostly in the hand and forearm  
193 muscles, contacts located at C7 level elicited triceps and contacts located at C5/C6 recruited  
194 biceps and deltoids (rostral). Those results were consistent in all animals (**Figure 2B, Extended**  
195 **Data Figure 3**). To ensure that this segmental selectivity translated into separate functional arm  
196 and hand movements, we delivered supra-threshold stimulation at various frequencies (20-120  
197 Hz) from each contact in two animals (Mk-Br and Mk-Yg). Indeed, since recruitment of  
198 motoneuron is pre-synaptic, EES may not be able to produce sustained muscle activation  
199 because of frequency dependent suppression<sup>60</sup>. This effect is an observed substantial  
200 suppression of muscle evoked potentials during repetitive stimulation of the afferents. Instead, we  
201 observed large and sustained arm movements during EES bursts. Muscle selectivity was  
202 preserved during long stimulation trains (**Figure 3C, F**) and different contacts elicited distinct  
203 functional joint movements (**Figure 3A, B, D, E, Video 1**) such as shoulder abduction, elbow  
204 extension and whole hand grasp. When looking at the energy of the EMGs, we found a monotonic  
205 relationship between muscle activation and stimulation frequency in most of the upper arm  
206 muscles (**Figure 3C, F**). However, not all muscles showed such clear frequency dependent  
207 responses (**Extended Data Figure 4A**). Moreover, peak-to-peak responses (**Extended Data**  
208 **Figure 4B**) were generally decreased during a burst at high frequency but were not abolished  
209 and tended to vary during the burst and while the movement was produced. We used these  
210 observations to optimize stimulation parameters to be used in a behavioral reach and grasp task  
211 (see Methods and **Extended Data Figure 5**). In summary, we found that single contacts of our  
212 spinal interface elicited segmental recruitment of arm flexors, extensors and hand flexors. Bursts  
213 of stimulation from these contacts produced sustained joint movements that were graded by  
214 stimulation frequency (**Extended Data Figure 6**).

215

216

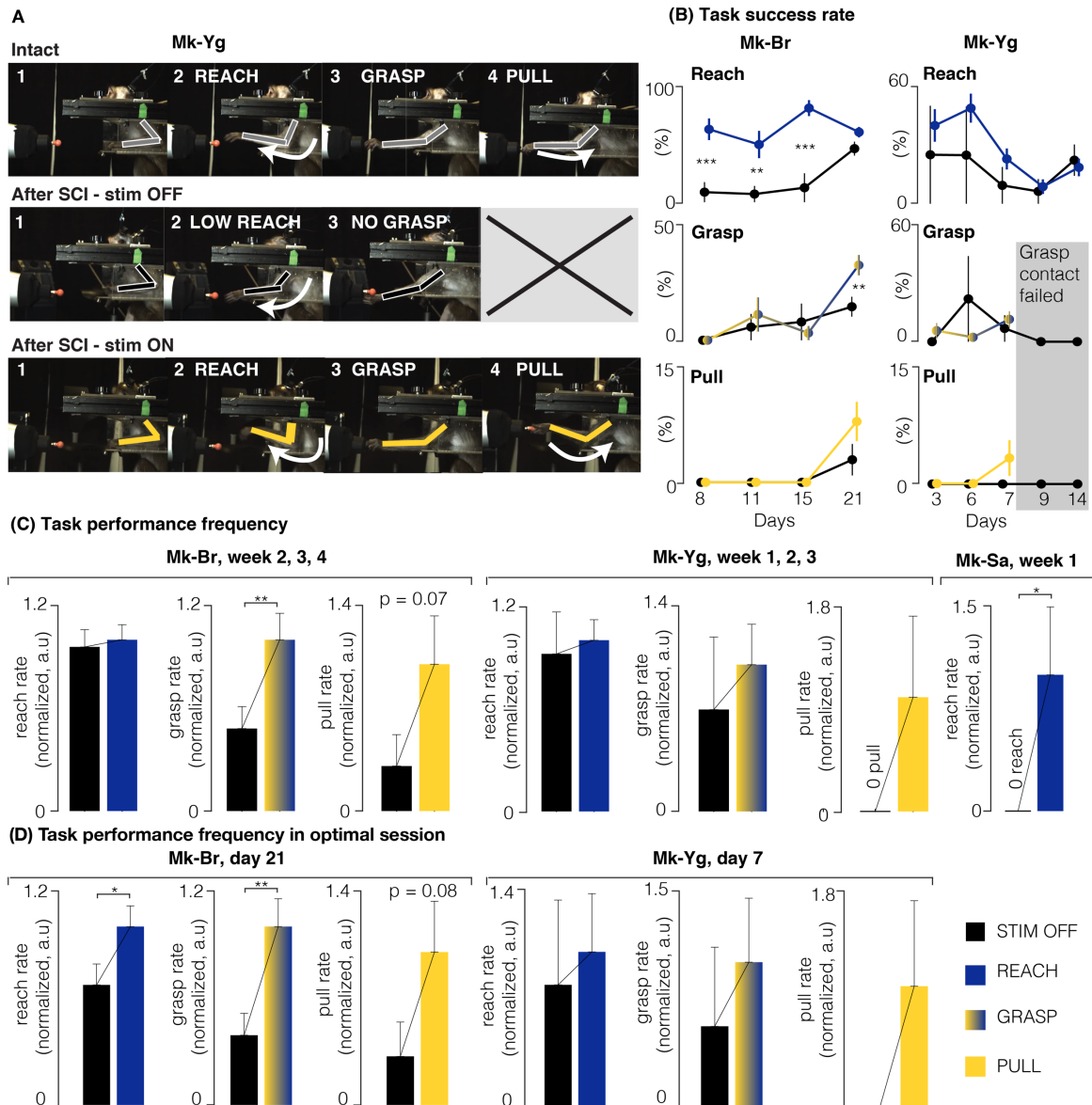


**Figure 4. EES improves task performance.** (A) Snapshots of Mk-Yg performing the task before SCI, after SCI without EES, and after SCI with EES. A full successful trial is composed of a reach, a grasp, and a pull. After SCI, Mk-Yg could only perform reaching movements without EES, while when EES was delivered the full task could be performed. (B) Task performance rate over all available sessions, computed as the percentage of successful movements across all attempted movements. Performance rate are shown for reach (blue), grasp (yellow to blue gradient) and pull (yellow movements). Data are shown as mean (bullets) and standard deviation (bars). Statistics was performed with Bootstrap. Asterisks: \* $p < 0.05$ , \*\* $p < 0.01$ , \*\*\* $p < 0.001$ . (C) Bar plots report the rate of successful movements after SCI without and with stimulation, for all the days in which animals performed the task. Rates were computed as number of successful trials per units of time. Data are presented as mean  $\pm$  STD and normalized on the mean value in stimulation condition. Statistics was performed with Bootstrap, Asterisks: \* $p < 0.05$ , \*\* $p < 0.01$ , \*\*\* $p < 0.001$ . (P-values. Mk-Br: reach, n.s; grasp,  $p = 0.01$ ; pull,  $p = 0.08$ . Mk-Yg: reach, grasp and pull n.s) (D) Bar plots report the rate of successful movements after SCI without and with stimulation, for the best session of Mk-Br and Mk-Yg. Data are presented as mean  $\pm$  STD and normalized on the mean value in stimulation condition. Statistics was performed with Bootstrap, Asterisks: \* $p < 0.05$ , \*\* $p < 0.01$ , \*\*\* $p < 0.001$ . (P-values. Mk-Br: reach,  $p = 0.04$ ; grasp,  $p = 0.002$ ; pull,  $p = 0.08$ . Mk-Yg: reach, grasp and pull n.s)



217

218 **Cervical EES substantially improves arm and hand motor function after spinal cord injury**

219 We next tested whether our stimulation protocol could improve functional outcomes of upper limb  
220 movements after SCI. Specifically, we tested the efficacy of EES to improve muscle activation,  
221 pulling forces, functional task performance, and kinematic quality of three-dimensional  
222 movements after SCI when stimulation was on against stimulation off as a control. In all monkeys,  
223 the lesion led to substantial motor deficits of the left arm and hand.

224 While each monkey retained the ability to activate proximal shoulder and biceps muscles, elbow  
225 extension and hand functions were severely compromised. Severity of the impairment and extent  
226 of spontaneous recovery (**Extended Data Figure 7**) varied across monkeys because of the  
227 variability in lesion size (**Figure 1E**). Generally, animals showed severe paralysis immediately  
228 after lesion, and then gradually regained some movement capabilities (**Extended Data Figure 7**).  
229 Due to the initial impairment, immediately after the lesion, monkeys were not able to perform the  
230 behavioral task. Consequently, during the first week, we simplified the task by presenting an  
231 object close to the monkeys and triggering stimulation bursts manually to encourage the animal  
232 to perform the task. After the first week, all monkeys spontaneously attempted to perform the task,  
233 making it possible to link the delivery of movement-specific stimulation bursts to real-time  
234 detection of movement onset using intra-cortical signals. Whenever the monkeys strived for a  
235 reach, grasp or pull movement, we delivered bursts of stimulation promoting reach or grasp/pull  
236 respectively (movement specific EES). Outcomes were computed for each animal independently  
237 and compared between EES on and EES off. In terms of functional task performances, without  
238 stimulation, the monkeys were rarely capable of completing any part of the task (defined as reach,  
239 grasp and pull). Instead, with the support of EES, both the percentage of success and the rate of  
240 success improved with rates that depended on the level of function of the animals over time. For  
241 example, reach was recovered immediately with larger improvements at the beginning, when  
242 deficits were larger in all three animals. Instead, improvements in grasps emerged only later when  
243 the animals spontaneously recovered some movement capacity (**Figure 4, Video 2,3,4**). More  
244 specifically Mk-Br improved grasp and pull only after 2 weeks with stimulation while Mk-Yg was  
245 never able to grasp and pull except during stimulation which we could test only until day 7 when  
246 the grasp contact E6 failed (see Methods). Instead, when we used our interface to deliver  
247 continuous EES that was not related to movement onsets, only non-significant and modest  
248 improvements were observed in Mk-Br while Mk-Yg did not show ability to grasp and pull during  
249 continuous EES (**Extended Data Figure 8A**). Moreover, we analyzed trials in which stimulation  
250 bursts were not triggered at movement onset, for example when pull stimulation was erroneously  
251 triggered during reach. In these trials the reach movement was abruptly interrupted, and the  
252 animal did not complete the task (**Extended Data Figure 8B, Video 5**).

253 During phase dependent stimulation, EES enhanced muscles activity and forces (**Figure 5A,B**)  
254 compared to no stimulation. In terms of movement quality, EES bursts triggered at movement  
255 onset significantly improved the overall quality of arm movements (**Figure 5B**). Indeed, principal  
256 component analysis (PCA) of three-dimensional kinematic parameters (i.e., timing, force, arm  
257 trajectories, joint angles) revealed that during EES, movement kinematics were significantly closer  
258 to pre-lesion kinematics than the few successful movements performed without stimulation  
259 (distance from pre-lesion performances in the multi-parametric kinematic space, **Figure 5B**).  
260 Notably, animals sustained the weight of the arm and lifted their elbow more, performed wider  
261 movements, and generated stronger forces (**Figure 5B**), getting closer to normal kinematic  
262 trajectory patterns without any long-term training.

263 In summary, we showed that EES bursts triggered at movement phase onsets, improved muscle  
264 strength, task performance and quality of arm movements. This allowed monkeys to perform  
265 reach, grasp and pull movements that were otherwise not able to perform without EES.

266

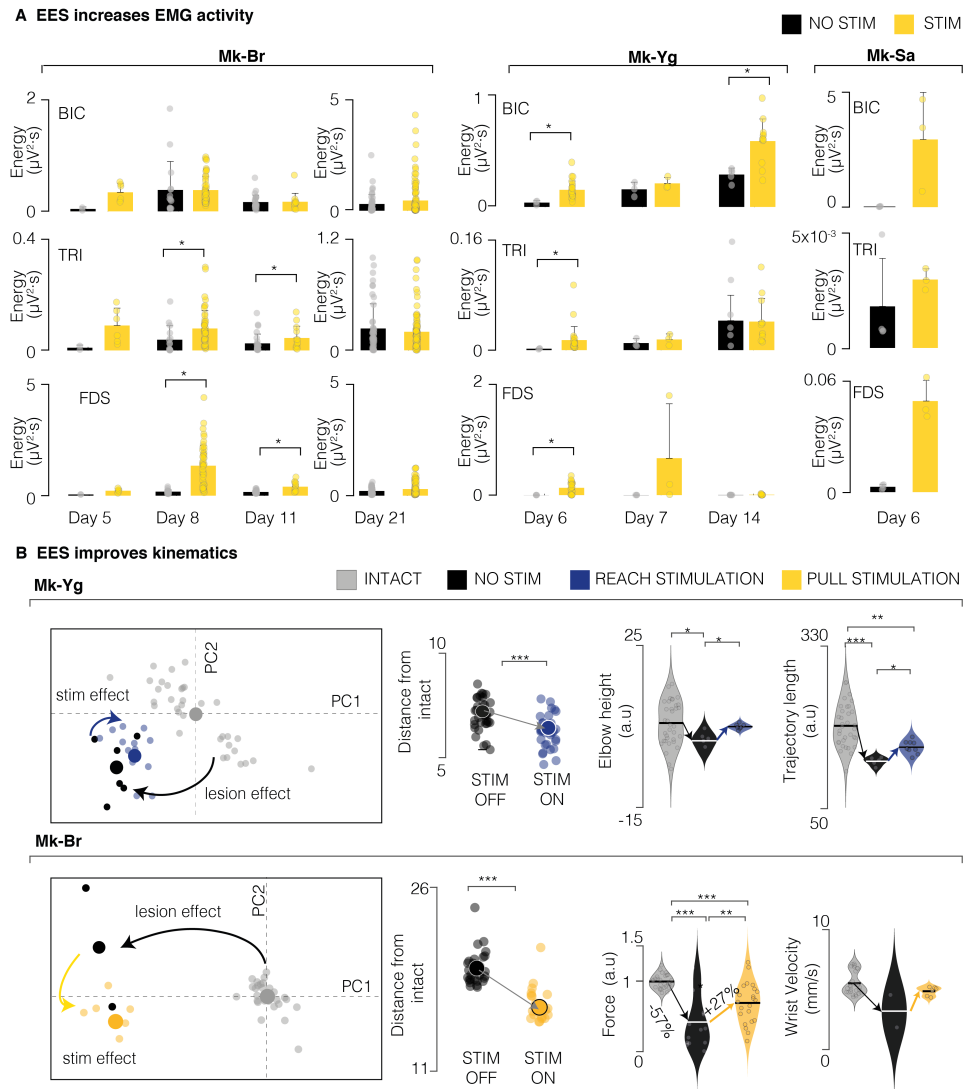


**Figure 5. EES improves muscle strength and movement quality. (A)** Bar plots of signal energy of biceps, triceps and FDS EMG profiles during movement with no stimulation (black) and stimulation (yellow). Data are shown for different sessions (one for each week) in Mk-Br and Mk-Yg. Mk-Sa performed only one session. All individual data points are represented by bullets. Statistical analysis with Wilcoxon Ranksum test. **(B)** PC analysis of kinematic features for Mk-Yg (top) and Mk-Br (bottom). From left to right: (1) first and second PC space. Each bullet represents one trial. Trials performed after injury (black) are consistently separated from the trials performed in intact conditions, highlighting a change in the quality of resulting kinematics. Trials performed with the support of stimulation (blue for reach and yellow for pull) are located closer to the intact trials in the PC space, denoting an improvement in kinematic features. (2) euclidean distance in the feature space of trials without stimulation (black) and with stimulation (blue for Mk-Yg, yellow for Mk-Br) from the centroid of the trials in intact condition; (3) example violin plots of movement quality features in the three conditions: intact, after SCI, and after SCI with stimulation. Statistics with Wilcoxon Ranksum test. Asterisks: \* $p < 0.05$ , \*\* $p < 0.01$ , \*\*\* $p < 0.001$ .

267

268

269

270

271  
272

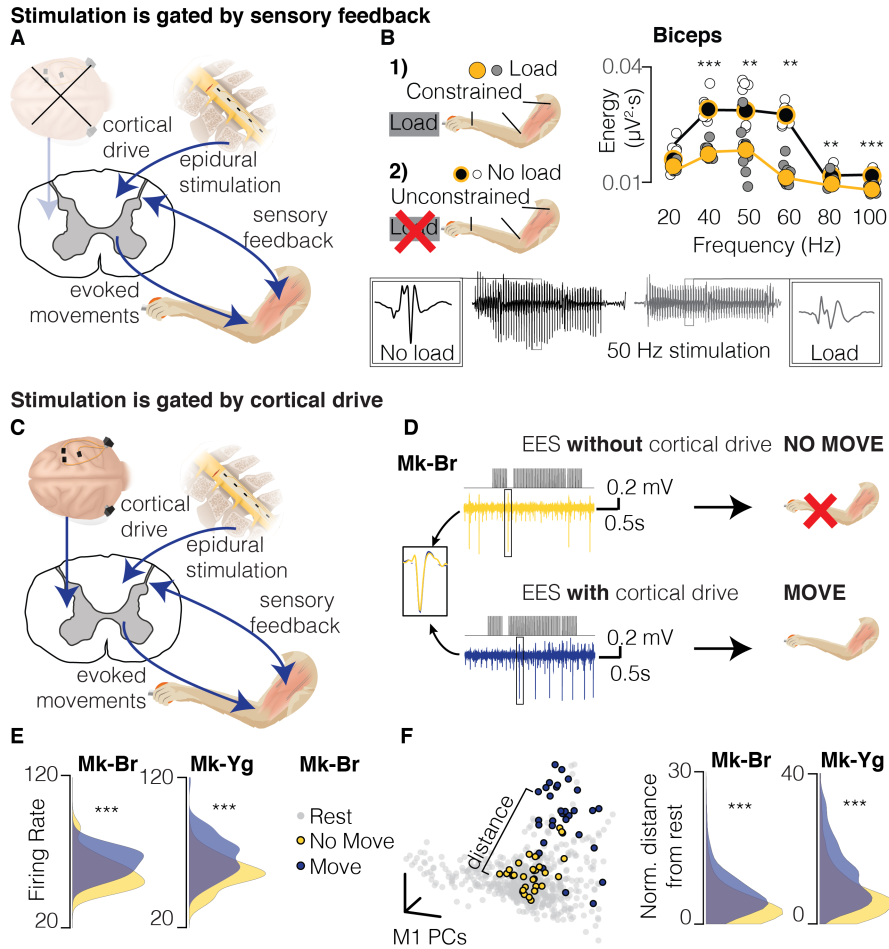


**Figure 6. EES must be synchronized with motor intention.** **(A)** Schematic of the interactions between EES and residual neural structures during anesthetized stimulation. During anesthesia, cortical control has no interaction, therefore EES interacts solely with sensory feedback spinal circuits. **(B)** Quantification of EMG activity during EES in two conditions: unconstrained arm (no load, black); arm constrained by load applied at the hand (load, gray). White and grey bullets: individual data points for no load and load conditions. Black and yellow bullets: mean values for no load and load conditions. Black and yellow lines: interpolation of mean values for no load and load conditions. On the bottom, example of EMG traces obtained during stimulation in the no-load (black) and load (gray) conditions. Stimulation artifacts have been removed. Data from Mk-Br **(C)** Schematic of interactions between EES and residual neural structures during the performance of the behavioral task. EES interacts with descending cortical drive sent through residual pathways after SCI, as well as with sensory spinal circuits. **(D)** Schematic illustrating the kinematic outcome of the interaction between EES and residual cortical inputs. The same EES pulse train (top) applied to Mk-Br can result in different motor outputs: no movement output when the cortex is silent (yellow, top), movement is produced when the cortex is active (blue, bottom). **(E)** Distribution of average firing rates across all M1 channels during stimulation trains that evoked no movement (yellow) and movement (blue). **(F)** Left: State space view of M1 activity for all time points during rest (gray), successful stimulation (blue) and unsuccessful stimulation (yellow). The brain states during unsuccessful stimulation (yellow) overlapped with the rest states, while the successful stimulation (blue) did not. Right: we computed a relative Mahalanobis distance between the two stimulation conditions and the cluster of neural states at rest. For both monkeys, neural states during stimulation periods with no movement were close to rest.

### 273 **Sensory inputs can decrease EES-induced motor output**

274 We then investigated the role of spinal circuits and sensory inputs in the production of the  
275 movements that we observed. Indeed, since activation of motoneurons was pre-synaptic, spinal  
276 reflexes and sensory inputs can influence EES evoked spinal reflexes in the legs<sup>22,61</sup>. In order to  
277 exclude influences of residual supraspinal voluntary inputs, we conducted experiments under  
278 propofol anesthesia (**Figure 6A**) with Mk-Br. We then delivered bursts of EES from the contact  
279 eliciting elbow flexion at varying stimulation frequencies in two distinct conditions (**Figure 6B**): in  
280 isometric and unconstrained conditions. In the isometric condition, we constrained the wrist, elbow  
281 and shoulder of the animal and measured force production at the wrist joint. Under unconstrained  
282 conditions we left the arm free to move under the effect of stimulation. This setup only differs from  
283 the sensory feedback generated at the load when pull forces are produced by EES. We found  
284 that EES induced EMG activity during unconstrained movement that was significantly different  
285 from the EMG activity induced during isometric movements (**Figure 6B**). In particular, overall  
286 EMGs and peak-to-peak amplitudes of elicited spinal reflexes were significantly lower when the  
287 arm was attached to a load (isometric) compared to when it was free to move. Albeit present at  
288 all frequencies, this difference was particularly important within the 40 to 60Hz range, thus  
289 overlapping with the functional frequency range that we selected for our study.  
290 These results show that force loads at the hand decreased EMG activity induced by EES as  
291 compared to no load applied at the hand. Under anesthesia, only changes on spinal circuit  
292 excitability induced by sensory inputs can explain the observed changes on EES evoked muscle  
293 activity.

### 294 295 **Some residual cortical input is necessary for cervical EES to be effective**

296 The influence of spinal sensory inputs showed that EES output may be decreased because of  
297 spinal sensory inputs when loads are applied at the hand. This would decrease the efficacy of  
298 EES which is supposed to enhance force production. Therefore, to explain the results we obtained  
299 in behaving monkeys (**Figure 6**) we investigated the contribution of residual cortical inputs in the  
300 production of forces and movements during EES. Specifically, since cortical inputs actively  
301 modulate spinal circuits, they should be able to both enhance and suppress EES output by  
302 modulating spinal circuit excitability<sup>30</sup>. Since we showed that monkeys could use EES to amplify  
303 their movement and forces (**Figure 6D**) we focused on demonstrating that cortical inputs could  
304 also suppress unwanted EES-generated movements. We hypothesized that if monkeys did not  
305 want to move, EES would not produce the large joint movements that we observed when the  
306 monkeys were anesthetized. Therefore, we identified trials in which our decoder detected a false-  
307 positive reach movement (**Figure 6C**). In this situation our system would deliver a burst of  
308 stimulation even if the animal was not attempting to execute the task. We then compared  
309 intracortical activity from the primary motor cortex (M1) of Mk-Br and Mk-Yg during these false-  
310 positive trials to the signals recorded during correctly detected trials. We identified trials where  
311 EES was present and the monkey moved, and trials when EES was present but the monkey did  
312 not move (**Figure 6D**). We verified that the same neural units were present in both conditions and  
313 found that the overall firing rates of all units in motor cortex was significantly higher when EES  
314 produced movement (**Figure 6E**) than when it did not. This suggested that movement happened  
315 only if the motor cortex was active, despite EES was delivered at amplitudes that generated large  
316 joint movements when the same monkey was anesthetized. To further validate this hypothesis  
317 we applied dimensionality reduction using Principal Component Analysis to the firing rates in each  
318 electrode and reduced the M1 population activity to low-dimensional states<sup>62</sup>. In this low-  
319 dimensional space each point represents the global neural state of the motor cortex at a given  
320 time point (**Figure 6F**). We compared the neural states present when EES was associated  
321 movements and those when EES was not associated movement with the neural states associated

322 to rest, e.g. when the monkeys were resting before the go signals between trial repetitions. When  
323 looking at the spatial distribution of neural states, trials in which EES was not associated to  
324 movement seemed to overlap with states of rest. We then computed the distance between each  
325 neural state to the subspace representing neural states at rest and found that the neural states  
326 associated to movements during EES were significantly further away from neural states at rest  
327 than neural states associated to EES and no movement. In summary, we found that the motor  
328 cortex activity was similar to the activity at rest whenever we delivered EES but the monkey did  
329 not move (**Figure 6F**). Instead, the monkey moved when the motor cortex was significantly active.  
330 This implies that the residual cortical inputs via direct and indirect pathway can either suppress  
331 or enable movement during EES.

332  
333

### 334 **Discussion**

335 We showed that EES of cervical spinal cord immediately enhanced muscle activation and strength,  
336 task performances and movement quality during a natural-like reach and grasp task in monkeys  
337 with unilateral cervical SCI compared to no stimulation controls in three monkeys. Importantly,  
338 our technique allowed monkeys to support the weight of their arm during reach, grasp and pull  
339 movements. These results are important in light of clinical translation of our technology. Stronger  
340 forces and better arm weight bearing can empower patients with the capacity to perform a larger  
341 spectrum of movements than they would normally be capable of doing without the need of support.  
342 This may provide for more independence in daily living as well as better outcomes of physical  
343 therapy.

344

### 345 **Exploiting subject-specific anatomy to simplify technology**

346 We obtained our results with relatively simple stimulation protocols that engaged up to three  
347 monopolar contacts (one for reach, one for grasp and one for pull). The combination of simple  
348 bursts through these contacts enabled whole arm multi-joint movements. We believe that the  
349 design of our interface was key to achieve this result. The dorsal roots are a robust anatomical  
350 target that we could easily identify through standard imaging to personalize surgical planning and  
351 interface design. A similar surgical planning approach can be imagined in humans where MRIs  
352 and CT can guide surgical planning<sup>51,63</sup>.

353 Our results were enabled by the relative mapping between each dorsal root and the rostral-caudal  
354 distribution of motoneurons in the cervical spinal cord, which is similar in monkeys and  
355 humans<sup>53,55,64</sup>. The anatomical separation of roots in the cervical enlargement allowed us to recruit  
356 each root independently which generated distinct joint movements to a degree that was not  
357 observed in applications of EES for the lower limbs<sup>49</sup>. Stimulation of the C6 root elicited distinct  
358 arm flexion, C7 stimulation produced arm extension and C8/T1 stimulation produced hand grasp.  
359 However, similarly to other spinal cord stimulation studies we could not identify contacts that  
360 selectively produced finger extension<sup>18,65,66</sup>. This is likely caused by the overlap of extensor motor-  
361 pools in the forearm<sup>55,64</sup> but possibly also because flexors may be biomechanically stronger and  
362 dominate hand kinematics in the case of co-contraction at rest. Despite these limitations in  
363 specificity, we were able to restore a whole three-dimensional arm movement by solely detecting  
364 movement onset signals to trigger pre-determined stimulation bursts through two or three contacts.  
365 Unlike FES, this is possible because EES activates cervical motoneurons via pre-synaptic inputs  
366 thus allowing modulation of elicited muscle responses that can compensate for reduced  
367 specificity<sup>30,49</sup>.

368

### 369 **Supporting arm movement phases independently**

370 Contrary to previous pilot applications of epidural and transcutaneous spinal cord stimulation of  
371 the cervical spinal cord<sup>35,36</sup>, we utilized a soft epidural interface that allowed selective and  
372 independent support of each movement phase rather than providing continuous stimulation to the  
373 whole spinal cord. This approach is not possible with transcutaneous technologies<sup>67</sup> or current  
374 design of human leads<sup>53</sup> and would require new interfaces designed for the cervical cord.  
375 Selective spatiotemporal stimulation was shown to be more effective in animal models and  
376 humans than continuous stimulation in the sense that it was able to immediately produce  
377 coordinated locomotion compared to continuous stimulation that instead required long training  
378 periods<sup>28,48,49,56</sup>. In the case of the upper limb we believe that this approach was critical. Indeed,  
379 while continuous stimulation did provide some level of facilitation, it failed to entirely promote  
380 grasp and pull in one of the monkeys. Perhaps the intrinsically unstructured nature of arm and  
381 hand control makes a continuous stimulation approach less effective than it is in locomotion that  
382 instead has an intrinsic repetitive structure<sup>38</sup>. For example, stimulation parameters that promote  
383 grasp, may impair reach if they are delivered continuously throughout movement. Indeed, when  
384 a pull stimulation was triggered at mid-reach it generated the interruption of the reach movement.  
385 Perhaps a different interface design or lower stimulation amplitudes could be used to optimize  
386 continuous stimulation protocols, but it would be at the expense of power of elicited movements  
387 potentially preventing the weight bearing component necessary for three-dimensional movements.  
388 In summary, the complex articulation of arm and hand movements may exacerbate the difference  
389 in efficacy between continuous and phase-specific stimulation protocols that was already  
390 observed for EES in locomotion, possibly explaining the difference in effect size that was obtained  
391 so far for application in the upper limb.

392

### 393 **The role of sensory feedback and residual cortical inputs in cervical EES**

394 We showed that sensory feedback when the hand was constrained to a force load reduced the  
395 EMG power produced by EES compared to free movements. This is likely caused by afferent  
396 inhibitory feedback coming from Ib afferents<sup>68</sup>. Unfortunately, lower muscle power while resisting  
397 a force load would decrease the clinical usability of this technology. We believe that this  
398 phenomenon is particularly relevant for the upper limb. Indeed, also during EES of the  
399 lumbosacral cord, the EES motor output is influenced by sensory inputs<sup>22,61</sup>, however sensory  
400 inputs are instrumental for locomotion and heavily contribute to the generation of the repetitive  
401 movement patterns that are required to walk<sup>16,22,23,38,69</sup>. Therefore, in the case of locomotion these  
402 inputs amplified and sustained EES-induced activity<sup>16,22,23,28</sup>. Instead arm and hand movements  
403 are produced by an unstructured sequence of primitive movements<sup>41</sup> and reflexes<sup>45</sup> in parallel  
404 with a sophisticated gating of sensory inputs through mechanisms such as pre-synaptic  
405 inhibition<sup>8,70</sup>. Therefore, residual cortical inputs become instrumental to obtain arm and hand  
406 movement with EES as shown by our analysis of intra-cortical signals during the production of  
407 movement combined with the observation that functional grasp was achieved only when the  
408 animals had recovered some level of function. Indeed, our lesions were non-complete and while  
409 most of the cortico-spinal tract was transected, multiple residual descending pathways were  
410 spared. These indirect inputs could have been used by the animals to mediate the inputs required  
411 to integrate EES and sensory inputs to produce voluntary movements. In summary, we believe  
412 that even during phase-specific EES residual cortical inputs play a critical role in enabling arm  
413 movement for cervical EES.

414

### 415 **Clinical significance and challenges**

416 The most important challenge for clinical translation of EES to humans concerns the role of  
417 residual inputs. Our data show that some level of residual inputs and of function is required to  
418 enable movement, first because in awake animals EES did not initiate movements, and second

419 because it lacks the selectivity to achieve selective finger activity. However, previous studies  
420 showed that even completely paralyzed subjects retain residual but functionally silent descending  
421 inputs<sup>25,32,51</sup>. Therefore, while overall efficacy may depend on injury severity, even severely injured  
422 patients may obtain benefits from cervical EES. After a period of physical training combined with  
423 EES<sup>71</sup> these subjects may be able to use EES to achieve simple but functional grasp. Alternatively,  
424 more selective technologies targeting hand muscles such as FES could be combined with EES  
425 to obtain powerful yet selective movements.

426 The adaptation of EMG output to stimulation frequency that we observed in consequence of pre-  
427 synaptic activation of motoneurons may lead to a reduction in efficacy during long-term clinical  
428 use. Additionally, stimulation of afferent fibers may cause uncontrolled reflexes which may affect  
429 function. While we did not observe these phenomena in our data, this may be due to the relatively  
430 small size of the lesion compared to severe contusion in humans. However, data in humans with  
431 SCI suggest that stimulation protocols can be adapted to be functional even in subjects with  
432 chronic severe thoracic lesions<sup>32,51</sup>, therefore we expect that this will be the case also for cervical  
433 lesions. At any rate both risks can be reduced by accurate stimulation tuning and real-time  
434 adaptation of stimulation patterns<sup>22,24,72</sup>.

435 Concerning complexity of our system, in our study we detected movement onsets from  
436 intracortical activity which may be seen as a limitation for a realistic implementation of our protocol  
437 in clinical settings. However, given the simplicity of our protocol which is essentially constituted  
438 by alternation of pre-defined bursts, brain recordings may not be required in clinics. Indeed, most  
439 patients suffer from a severe but incomplete paralysis<sup>51,73</sup>, which spares some residual muscle  
440 activity in few muscles. While this residual activity is not sufficient to produce functional  
441 movements, it can be reliably detected and used to trigger stimulation bursts with standard clinical  
442 technologies<sup>49,51</sup>. In summary, we believe that by exploiting the functionality of residual spinal  
443 circuits and supra-spinal inputs, cervical EES constitutes a simple yet robust approach to the  
444 restoration of arm motor control with significant translational potential.

445

#### 446 **Acknowledgements**

447 The authors would like to thank Jacques Maillard and Laurent Bossy for the care provided to the  
448 animals, Dr Eric Schmidlin and Dr Simon Borgognon for their help with anaesthesia and surgery  
449 preparations, Dr Marion Badi for her help and advice during experiment preparations and  
450 experimental procedures, Dr. Andrina Zbinden for her contribution to the health survey of the  
451 monkeys, André Gaillard and Andrea Francovich for their help with the implementation of the  
452 hardware and the students of the University of Fribourg Amélie Jeanneret, Alen Jelusic, Laora  
453 Marie Jacquemet and Samia Borra for their help in processing data.

454

#### 455 **Funding**

456 The authors would like to acknowledge the financial support from the Wyss Center grant (WCP  
457 008) to MC, GC and TM, an industrial grant from GTX medicals to GC and MC; the Bertarelli  
458 Foundation (Catalyst Fund Grant to MC and TM and funds to SL) a Swiss National Science  
459 Foundation Ambizione Fellowship (No. 167912 to MC), a Swiss National Science Foundation  
460 Doc-Mobilit Grant to BB, The European Union's Horizon 2020 research and innovation program  
461 under the Marie Skłodowska-Curie grant agreement no. 665667 (GS) the Swiss National  
462 foundation grant BSCGIO\_157800 (SL), a Whitaker International Scholars Program fellowship to  
463 MGP, and an internal pilot grant of the University of Fribourg to MC.

464

#### 465 **Author Contributions**

466 MC, BB and SC conceived the study; BB, MGP, and TM designed and implemented the hardware  
467 and software tools; SC designed the behavioral task and training strategy; GS and SL designed  
468 and manufactured the implantable interface; BB, SC, MGP and MC conducted the experiments;  
469 BB, SC, MGP and KZ performed the data analysis; SC, MD and MK trained the animals; SC, KG,  
470 NJ and QB processed the histological data; JB, GC and MC designed surgical implantation  
471 strategies and stimulation strategies. GC and JB, performed surgical implantations and lesions.  
472 EMR and MC implemented and supervised procedures on monkeys; MC, BB, SC and MGP wrote  
473 the manuscript; all authors edited the manuscript; SL, TM, JB, GC and MC secured funding for  
474 the study; MC supervised the study.

475

#### 476 **Competing Interests**

477 G.C., J.B., S.L., M.C., B.B. and K.Z. hold various patents in relation to the present work. G.C.,  
478 S.L. and J.B. are founders and shareholders of GTX medical, a company developing an EES-  
479 based therapy to restore movement after spinal cord injury.

480

#### 481 **Data and materials availability**

482 All software and data will be available upon reasonable request to the corresponding author.

483

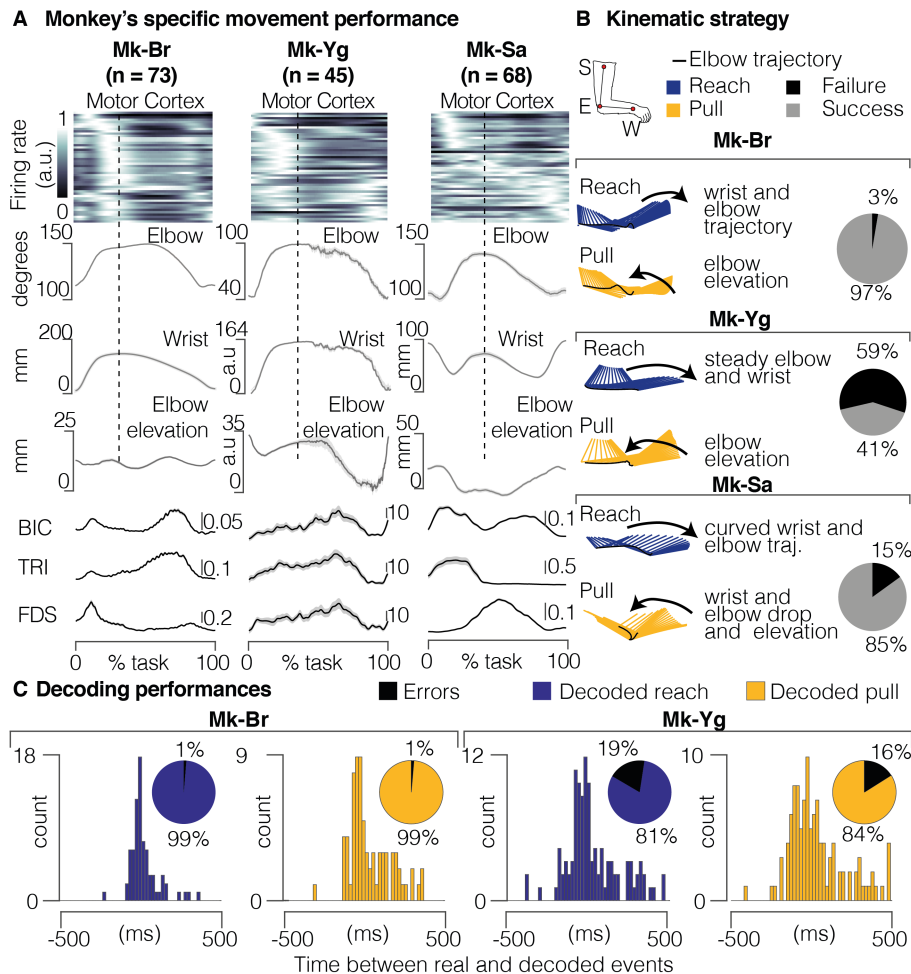
484

485

486

487

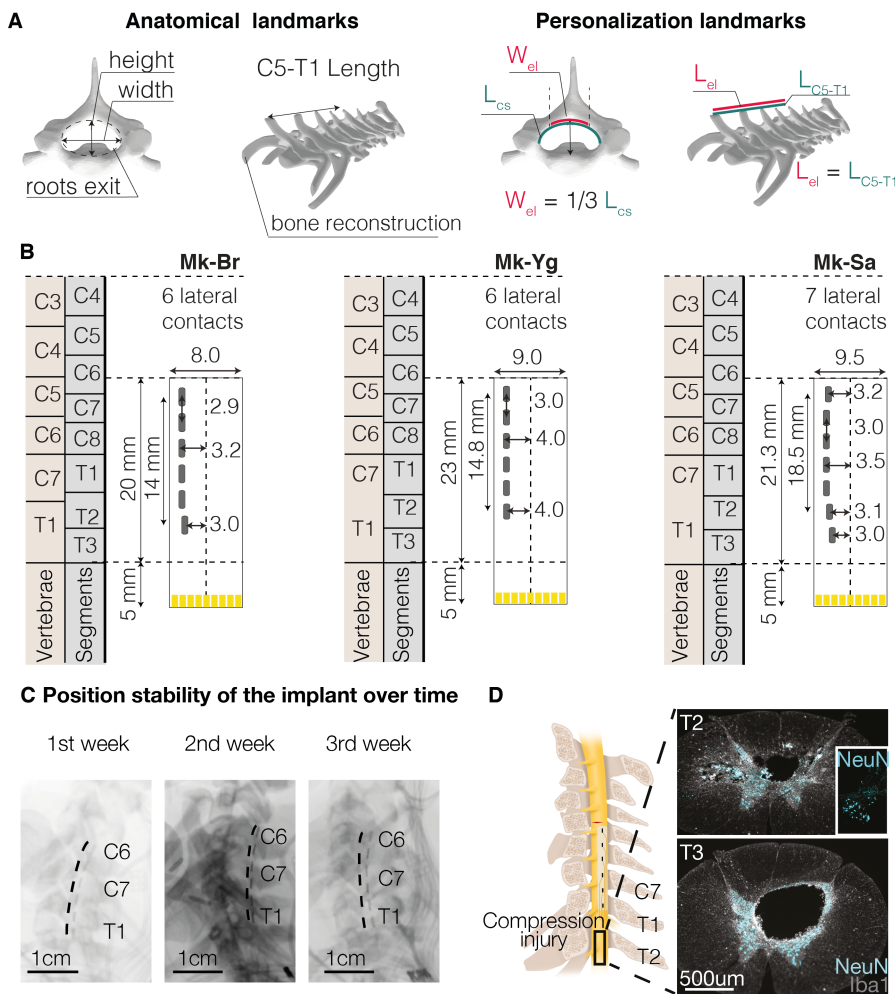




**Extended Data Figure 1. (A)** Portfolio of signals recorded during intact movement for each animal. These signals have been recorded during the experimental session prior to the lesion. Motor cortex recordings show firing rate profiles for the 64 microelectrodes. Each row shows the firing rate of a specific electrode. Electrodes are displayed from top to bottom by order of first activation in a reference trial. Arbitrary units in motor cortex recording indicate normalized firing rate for each electrode (see methods). In kinematic and EMG plots, black lines correspond to the mean profile across all trials, shaded area shows the SEM across all trials. Kinematic scales are expressed in mm. For Mk-Yg, arbitrary units on kinematic plots represent displacement units derived by the count of video pixels. EMG scales are expressed in mV. **(B)** Kinematic strategies implemented by each monkey. Stick diagrams representations of the arm kinematic during reach (blue) and pull (yellow). The black line highlights the elbow trajectory. Pie charts represent the percentage of success and failure in task performance before lesion. **(C)** Offline decoding performance for Mk-Br and Mk-Yg before lesion. Histograms show timing accuracy of reach (blue) and pull (yellow) event decoding. The height of bars (y coordinate) illustrates the amount of events decoded with a specific timing accuracy (x coordinate). Pie charts (inset) show the percentage of correctly identified (true positive) reaches (blue) and pulls (yellow), across all decoded events. The black portion of the pie chart highlights the percentage of false positive decoded events.

489

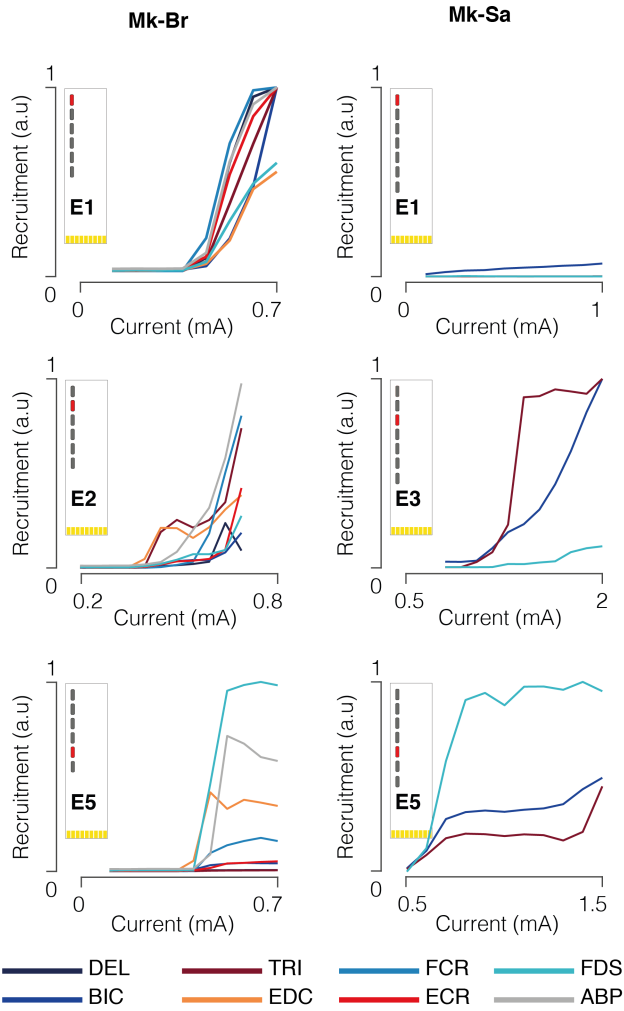
490



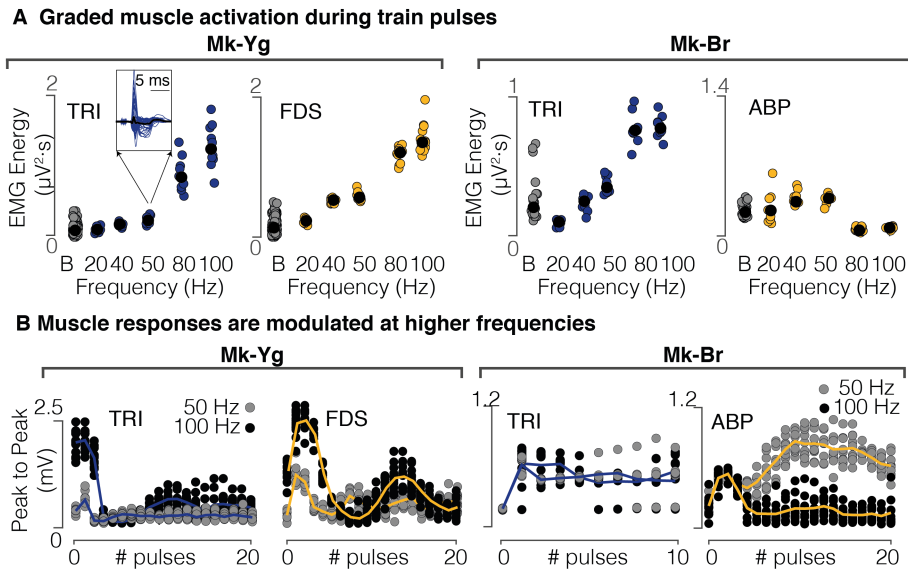
491

492

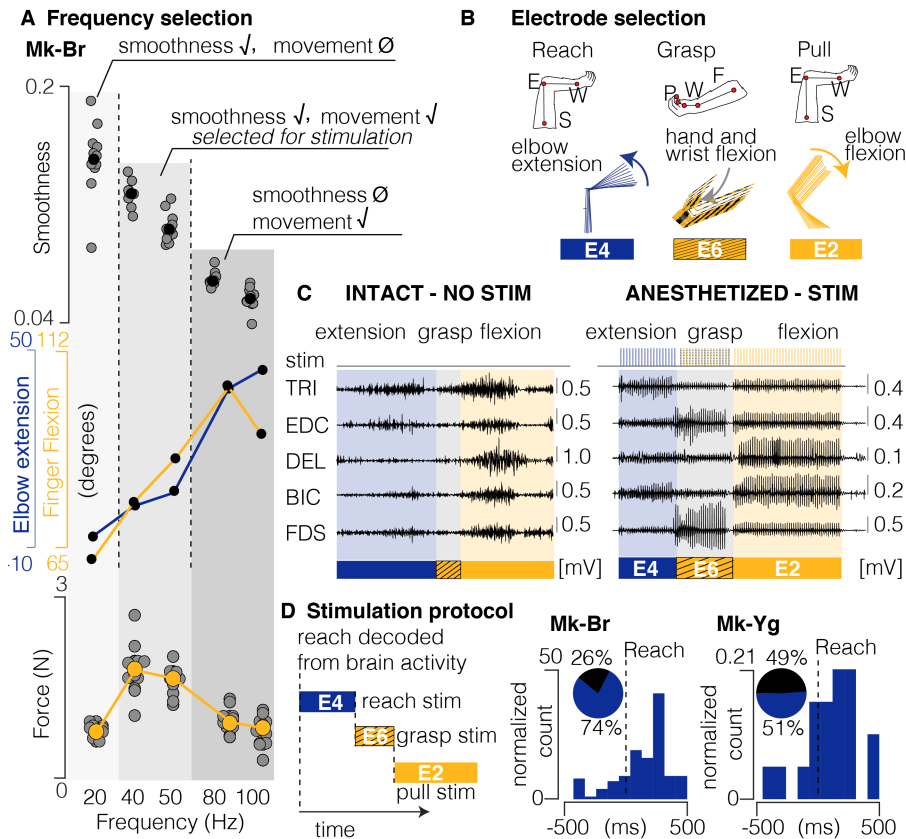
### Recruitment curves



**Extended Data Figure 3.** Muscle recruitment obtained by stimulating (1 Hz) at C5, C6/C7, and T1 spinal segments for Mk-Br and Mk-Sa. Mk-Sa only had three muscles implanted: biceps, triceps, and flexor digitorum superficialis.

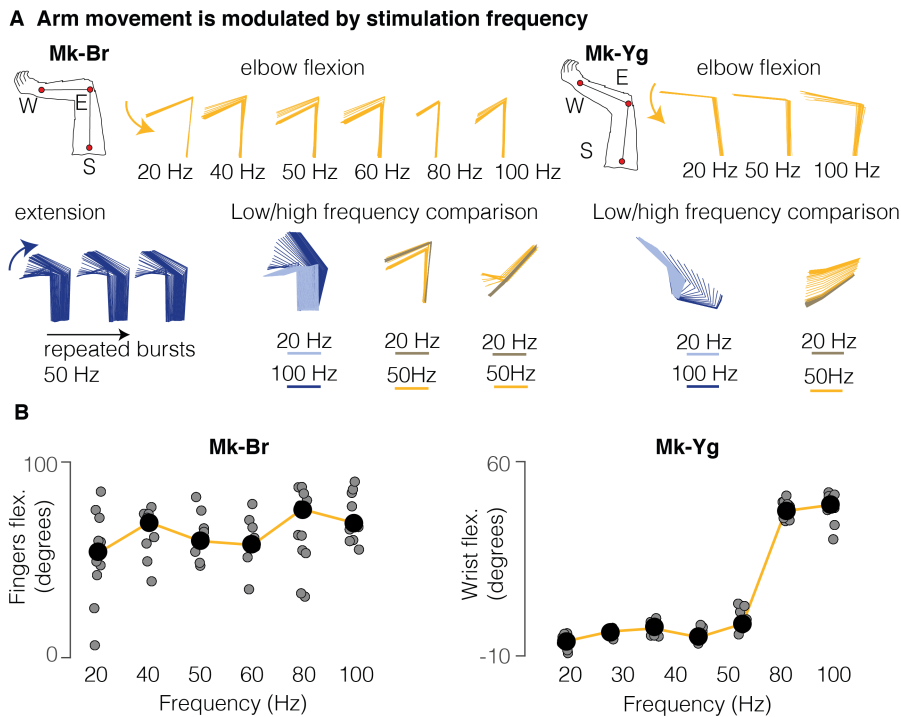


**Extended Data Figure 4. (A)** Energy of EMG signals of triceps (Mk-Br and Mk-Yg), Flexor Digitorum Superficialis (Mk-Yg) and abductor pollicis (Mk-Br) muscles, following pulse-train stimulation at different frequencies (on the x-axis). Black bullets represent mean values. **(B)** Evolution over time of the peak-to-peak value of stimulation evoked responses during a stimulation burst. Each plot shows the evolution for a specific muscle following pulse-train stimulation at 50 and 100Hz. Triceps is shown for Mk-Br and Mk-Yg, Flexor Digitorum Superficialis for Mk-Yg and abductor pollicis for Mk-Br. Each data point is represented as a bullet and lines represent mean values over time.



**Extended Data Figure 5. Design of stimulation protocol.** (A) Combined representation of movement smoothness, elbow and finger flexion, and pulling force during anesthetized stimulation. Shades of gray highlight three frequency ranges that produce: (1) smooth trajectory, but little movement and low force (20Hz), (2) smooth trajectory, extended movement and medium force (40 and 50Hz), (3) abrupt and very extended movement and low force (80 and 100Hz). Kinematics and force reported here were measured in different experiments, kinematics was unconstrained, force data were acquired in isometric conditions (see Methods). The range 40-50 Hz was selected as the best optimization of sufficient movement, smoothness and force production. (B) Schematic representation of arm and hand kinematics during stimulation delivered from the selection of three contacts to produce elbow extension (blue), hand and wrist flexion (yellow and black), and elbow flexion (yellow). (C) Example of comparison between EMG activity during intact movement (left) and movement elicited by chaining stimulation from the three selected contacts (right). (D) Scheme illustrating how stimulation is triggered from movement-related intra-cortical signals. On the right, online performances of movement attempt decoder in two animals with SCI. Pie charts represent percentage of predicted (blue) and unpredicted (black) reach events by our decoder.

496

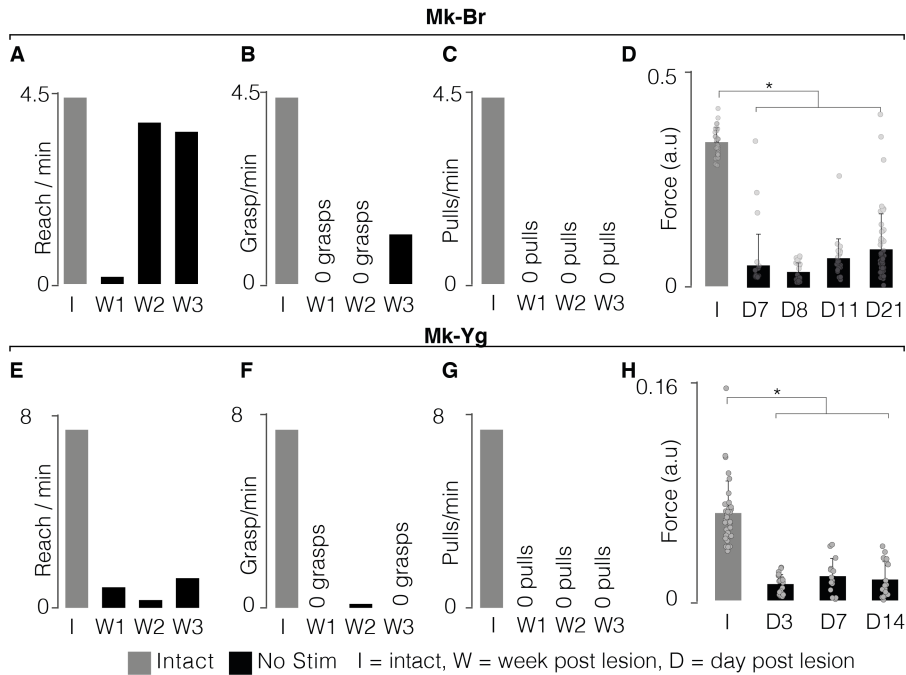


**Extended Data Figure 6. (A)** Stick diagram schematic of movements elicited by pulse-trains of stimulation in anesthetized conditions. Mk-Br: on the left, arm kinematic obtained by delivering stimulation at different frequencies from contact number 5, on the bottom-left, arm kinematics obtained by repetitive delivery of a burst at 50 Hz; on the bottom right, superimposition of stick diagrams obtained with stimulation at 20 Hz and at higher frequencies (50 or 100 Hz) from different contacts. For Mk-Yg: arm kinematic obtained by delivering stimulation at different frequencies from contact number 2 and superimposition of stick diagrams obtained with stimulation at 20 Hz and at higher frequencies (50 or 100 Hz) from different contacts. **(B)** On the left, finger flexion produced by stimulation at different frequencies from the grasp contact in Mk-Br. Black bullets represent the mean value across different pulse-trains. On the right, wrist flexion obtained by stimulation at different frequencies from the grasp contact in Mk-Yg.

497

498

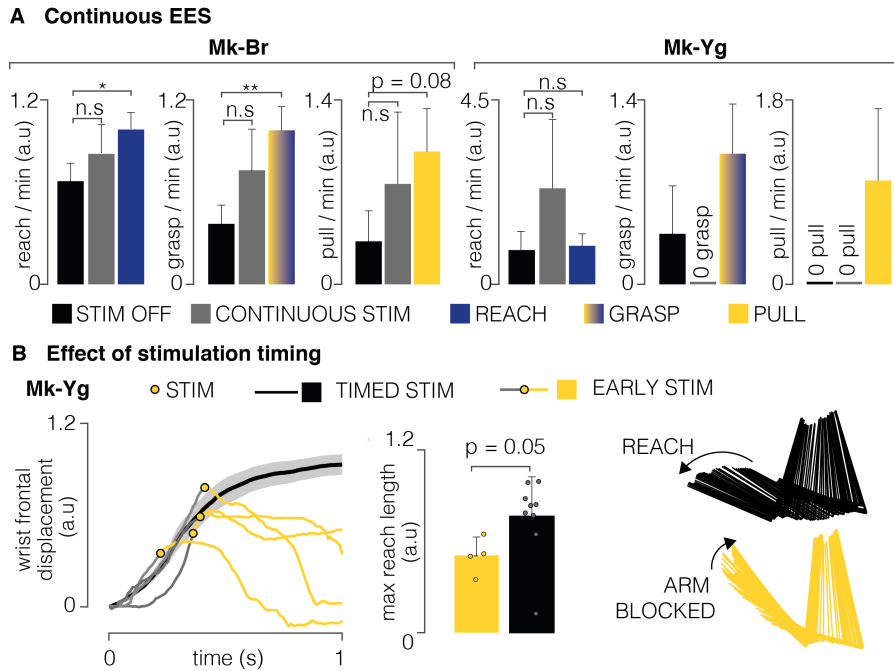
499



**Extended Data Figure 7. (A)** Evolution (in weeks) of rates at which Mk-Br performed reach movements after SCI (black), compared to the performances before injury (gray). **(B)** Evolution (in weeks) of rates at which Mk-Br performed grasp movements after SCI (black), compared to the performances before injury (gray). **(C)** Evolution (in weeks) of rates at which Mk-Br performed pull movements after SCI (black), compared to the performances before injury (gray). **(D)** Evolution (in days) of pull force after SCI without stimulation for Mk-Br. Values are plotted as the mean  $\pm$  SEM. Statistical analysis was carried out with Wilcoxon Ranksum test. **(E)** Evolution (in weeks) of rates at which Mk-Yg performed reach movements after SCI (black), compared to the performances before injury (gray). **(F)** Evolution (in weeks) of rates at which Mk-Yg performed grasp movements after SCI (black), compared to the performances before injury (gray). **(G)** Evolution (in weeks) of rates at which Mk-Yg performed pull movements after SCI (black), compared to the performances before injury (gray). **(H)** Evolution (in days) of pull force after SCI without stimulation for Mk-Yg. Values are plotted as the mean  $\pm$  SEM. Statistical analysis was carried out with Wilcoxon Ranksum test.

500

501



**Extended Data Figure 8. (A)** Bar plots report the rate of successful movements after SCI, without stimulation (black), with continuous stimulation (gray) and with phase-dependent stimulation (blue or yellow) for Mk-Br and Mk-Yg. Data are presented as mean  $\pm$  STD and normalized on the mean value in stimulation condition. Statistics was performed with Bootstrap. **(B)** Left: wrist frontal displacement in trials in which pull stimulation was erroneously triggered during reach (gray and yellow), compared to trials in which pull stimulation was not delivered (black). Yellow bullets highlight the instant at which stimulation was delivered: yellow lines highlight the trajectories during and after stimulation. Middle: barplot of the length of the reach movement when pull stimulation was erroneously delivered and when pull stimulation was not delivered. Data are presented as mean  $\pm$  STD. Right: stick diagram of arm kinematics during reach without (black) and with (yellow) erroneous pull stimulation.

502



## 503 **Materials and Methods**

504

### 505 Animals involved in the study

506

507 All procedures were carried out in accordance to the Guide for Care and Use of Laboratory  
508 Animals<sup>74</sup> and the principle of the 3Rs. Protocols were approved by local veterinary authorities of  
509 the Canton of Fribourg (veterinary authorization No 2017\_04\_FR and 2017\_04E\_FR), including  
510 the ethical assessment by the local (cantonal) Survey Committee on Animal Experimentation and  
511 final acceptance by the Federal Veterinary Office (BVET, Bern, Switzerland). Three adult female  
512 *Macaca Fascicularis* monkeys were involved in the study (Mk-Sa 9 years old, 4.0 kg, Mk-Br 3  
513 years old, 3.4 kg, Mk-Yg 3 years old, 4.0 kg). Animals were not food deprived, could freely access  
514 water at any time and were housed in collective rooms designed in accordance to the Swiss  
515 guidelines (detention in groups of 2-5 animals in a room of at least 45 m<sup>3</sup>). Rooms were enriched  
516 with toys, food puzzles, tree branches and devices to climb and hide, as well as access to an  
517 outdoor space of 10-12 m<sup>3</sup> (see [www.unifr.ch/spccr/about/housing](http://www.unifr.ch/spccr/about/housing)). Detailed information on which  
518 animals were involved in specific experimental procedures are reported in **Supplementary Table**  
519 **1**.

### 520 Surgical procedures

521 For each animal, we performed three surgical procedures, (1) intracortical electrodes implantation,  
522 (2) intramuscular electrodes implantation, and (3) epidural implant insertion and spinal cord injury.  
523 Mk-Sa deviated from this protocol. Mk-Sa was first implanted with the epidural interface before  
524 injury, however an infection occurred and resulted in the explanation of the lead to treat the  
525 infection. After recovery, the animal was re-implanted, and lesion performed following the same  
526 protocol of Mk-Br and Mk-Yg. All the surgical procedures were performed under full anaesthesia  
527 induced with midazolam (0.1 mg/kg, i.m.), methadone (0.2 mg/kg, i.m.), and ketamine (10 mg/kg,  
528 i.m.) and maintained under continuous intravenous infusion of propofol (5 ml/kg/h) and fentanyl  
529 (0.2-1.7 ml/kg/h) using standard aseptic techniques. A certified neurosurgeon (Dr. Jocelyne Bloch,  
530 CHUV, Lausanne, Switzerland) performed all the surgical procedures.

531 During the first surgical procedure, we implanted multi-microelectrode arrays in the primary motor  
532 cortex (M1-42 channels), ventral premotor cortex (PMv-32 channels) and primary somatosensory  
533 cortex (S1-42 channels) for a total of 128 channels for Mk-Br and Mk-Yg (Blackrock Microsystems,  
534 400  $\mu$ m pitch and electrodes tip lengths 1.5 mm 1.5 mm and 1mm for M1, PMv and S1  
535 respectively). Instead, Mk-Sa was implanted with 2 microelectrode arrays of 64 channels each  
536 and pitch of 1.5 and 1 mm in M1 and PMd respectively. Functional motor areas of the arm were  
537 identified through anatomical landmarks and intra-surgical micro-stimulation. In order to access  
538 the brain areas of interest we performed a 20 mm diameter craniotomy and we incised the dura.  
539 The arrays implantation was achieved using a pneumatic compressor system (Impactor System,  
540 Blackrock Microsystems). A pedestal (*Pedestal A*) was then fixated to a compliant titanium mesh  
541 (Medtronic Ti-Mesh) modelled to fit the skull shape and implanted in a previous surgery a few  
542 weeks earlier<sup>54</sup>.

543 During the second surgical procedure we implanted intramuscular electrodes (Teflon-coated  
544 stainless-steel wires, Cooner Wire, cat. no. AS631). Mk-Yg received electrodes in the following  
545 arm and hand muscles: Deltoid (DEL), Biceps Brachii (BIC), Triceps Brachii (TRI), Extensor  
546 Digitorum Communis (EDC), Flexor Carpi Radialis (FCR), Extensor Carpi Radialis (ECR), Flexor  
547 Digitorum Superficialis (FDS). Mk-Br received an additional electrode in the Abductor Pollicis

548 Brevis (ABP). Due to practical constraints, Mk-Sa received electrodes only in Biceps Brachii (BIC),  
549 Triceps Brachii (TRI) and Flexor Digitorum Superficialis (FDS). In all animals, wires were then  
550 connected to an additional pedestal (Pedestal B), fixated to the titanium mesh.

551 During the third surgical procedure, monkeys were subjected to a lesion at the cervical level  
552 (C5/C6) of the spinal cord. The surgeon used a micro-blade to cut approximately one third of the  
553 dorsolateral aspect of the spinal cord, in order to interrupt the main component of the corticospinal  
554 tract unilaterally. All monkeys retained autonomic functions, as well as limited arm flexion and  
555 shoulder adduction capabilities. We monitored the animals for the first hours after surgery and  
556 several times daily during the following days. Monitoring scales (score sheets) were used to  
557 assess post-operative pain and general health condition during 1-2 weeks. Antibiotics were given  
558 immediately after the surgery and then once per day for 10 subsequent days, anti-inflammatory  
559 drugs were given once per day for 5 days (Rymadyl 4mg/kg, s.c.; Dexamethasone 0.3mg/kg, s.c.),  
560 and analgesic was given twice per day for 5 days (Temgesic 0.01mg/kg, i.m.). Within the same  
561 procedure, each monkey received a tailored epidural implant. The implant was inserted in the  
562 epidural space of the cervical spinal cord, according to methods described in Schiavone 2020<sup>57</sup>  
563 and Capogrosso 2018<sup>49</sup>. The implant was inserted below the T1 vertebra and pulled until it  
564 covered spinal segments from C6 to T1. We performed intra-operative electrophysiology in order  
565 to assess and refine the implant positioning so that electrodes are aligned to the animal-specific  
566 anatomical features. In particular, we verified that single pulses of stimulation delivered from the  
567 most rostral and most caudal electrodes elicited contractions in the BIC and FDS muscles  
568 respectively. We re-routed the wires subcutaneously in order to connect them to the *Pedestal B*.  
569 All surgical and post-operative care procedures were developed in details in previous reports<sup>49,50</sup>.

#### 570 Data acquisition

571 For Mk-Sa and Mk-Br, we acquired three-dimensional spatial coordinates of arm and hand joints  
572 using a 14-camera motion tracking system (Figure 1, Vicon Motion Systems, Oxford, UK) that  
573 tracked the Cartesian position of 6 infrared reflective markers (6 to 9 mm in diameter each, Vicon  
574 Motion Systems, Oxford, UK) at a 100 Hz framerate. All markers were placed on the left arm, one  
575 below the shoulder, three on the elbow (proximal, medial and distal position), and two on the left  
576 and right side of the wrist. For each subject, a model of the marker placement was calibrated in  
577 Vicon's Nexus software at the beginning of each experimental session. For Mk-Yg spatial  
578 coordinates of arm and hand joints were recorded using two cameras placed parallel to the sagittal  
579 and transversal plane of the animal (Vicon Motion Systems, Oxford, UK). The 3D coordinates of  
580 the arm and hand joints were extracted using DeepLabCut<sup>75</sup>. Due to the reduced informative  
581 content extracted from the camera parallel to the transverse plane, we then only used 2D  
582 coordinates on the animals' sagittal plane. The training set needed for automatic data labeling  
583 was created by manually labeling a subset of recorded videos. An investigator was blinded to the  
584 experimental condition and was instructed to mark four anatomical landmarks that mirrored the  
585 position of markers in Mk-Sa and Mk-Br (shoulder, medial elbow, left and right wrist). Neural  
586 signals were acquired with a Neural Signal Processor (Blackrock Microsystems, USA) using the  
587 Cereplex-E headstage with a sampling frequency of 30 kHz. Electromyographic signals were  
588 acquired with a Behavioral Neurophysiology chronic recording system (RZ2 BioAmp Processor,  
589 Tucker-Davis Technologies, USA) at a sampling frequency of 12207 Hz.

590

#### 591 Electrophysiology in sedated monkeys

592 Monkeys were sedated with a continuous intravenous infusion of propofol (5 ml/kg/h) that  
593 minimizes effects on spinal cord stimulation<sup>76</sup>. We delivered single pulses of cathodic, charge  
594 balanced, asymmetric square pulses (0.3 ms, 1 Hz) from each electrode contact while recording  
595 compound potentials from all implanted arm and hand muscles. Electromyographic signals were  
596 acquired with a Behavioral Neurophysiology chronic recording system (RZ2 BioAmp Processor,  
597 Tucker-Davis Technologies, USA) at a sampling frequency of 12207 Hz. We then delivered 10  
598 repetitions of pulse trains from each contact, at several frequencies ranging from 20 to 120 Hz.  
599 We recorded compound potentials from all implanted arm and hand muscles and arm kinematics  
600 through two high resolution cameras (Sony FDR-X3000 Action Cam 4K). Through this procedure  
601 we identified three contacts that primarily elicited (1) arm flexors, (2) arm extensors and (3) hand  
602 flexors. In a reduced set of trials, we also recorded the force produced by arm flexion through a  
603 10 N range force sensor (Dual-Range Force Sensor, DFS-BTA, Vernier, Beaverton, Oregon,  
604 USA). To record the pulling force produced during isometric arm flexion, the hand was fixated to  
605 the sensor hook through a string, and the sensor and the elbow were kept in place by two  
606 experimenters, in order to optimally capture the strength produced by muscle contraction.

### 607 Behavioral experimental recordings

608 All animals were trained to perform a three-dimensional robotic reach, grasp and pull task,  
609 previously described in detail in (Barra 2019<sup>54</sup>) and briefly recalled here for simplicity.  
610 All animals were instructed to wait for a start signal by resting the left hand on a metallic bar.  
611 When the “go-cue” was given, monkeys had to reach for and grasp a small spherical object  
612 attached to the robot end effector and located in the three-dimensional space. The object was  
613 placed approximately 180 mm above the animal seating height, 150 mm far from the  
614 shoulder/head coronal plane and 30 mm left of the animal’s left arm. Once animals got a hold on  
615 the object, they had to pull it towards their own body until trespassing a virtual spatial threshold.  
616 The accomplishment of such virtual threshold was automatically detected by the robot control  
617 through online monitoring of the end effector position. Once attained the threshold, monkeys had  
618 to let go on the object and go back to the metallic bar. Fruits and vegetables were used to reward  
619 successful movements. Animals were trained daily (5 days per week) and every session ended  
620 as soon as the animals showed any sign of fatigue or impatience.

621 For Mk-Sa, data presented in this paper were collected several weeks pre lesion and 1 week post  
622 lesion, unfortunately a severe infection of the spinal array and EMGs that recurred after day 7  
623 lead to the premature euthanasia of the monkey before the study could be completed, in  
624 agreement with the endpoints in our veterinary authorization. For Mk-Br and Mk-Yg data  
625 presented in this paper were collected several weeks pre lesion and until 3 weeks post lesion. At  
626 the end of week 3 post lesion, Mk-Br had 2 episodes of self-mutilation on the foot ipsi-lateral to  
627 the lesion. In consequence we euthanized the animal before the end of the protocol according to  
628 the endpoints in our veterinary authorization. As described in the results section, we found post-  
629 mortem that Mk-Br had a medial spinal cord contusion at the T3 level. While this lesion did not  
630 affect motor control of the legs or the arms, it may have generated neuropathic pain. Mk-Yg could  
631 perform the entire protocol without any adverse event, however after day 7, the caudal contact of  
632 the spinal interface (E8) identified to promote grasp failed, thus preventing us to perform  
633 experiments with optimal stimulation configuration and impacting the efficacy of grasp movements.

634

635

636 *Optimization of EES parameters*

637 To optimized stimulation parameters we exploited the frequency/kinematic relationship that we  
638 observed during single contact stimulation (**Figure 3B,E**). We then analyzed single joint  
639 movements at different frequencies and contacts and weighted joint excursion angles against  
640 movement smoothness<sup>77</sup>, we found that stimulation frequencies of 50-60 Hz (**Extended Data**  
641 **Figure 5**) produced smooth<sup>77</sup> and full-range movements and maximal forces. Instead, movements  
642 elicited at frequencies lower than 40 Hz were too weak to complete a full joint movement while  
643 frequencies higher than 60 Hz produced either abrupt movements or incomplete movements  
644 (**Extended Data Figure 5A**). Next, we identified among all the tested contacts, those that could  
645 consistently elicit arm extension (reach), hand flexion (grasp) and arm flexion (pull) (**Extended**  
646 **Data Figure 5B**). We chose these contacts and 50-60Hz to sustain full arm and hand movement  
647 and tested their effect in anesthetized animals by sequentially executing bursts on each of these  
648 three contacts. We verified that the sequence triggered whole arm and hand movements that  
649 mimicked smooth<sup>77</sup> and natural multi-joints movements (**Extended Data Figure 5C, Video 1**).  
650 Specifically, extension, grasping and pulling movements produced clear EMG bursts as well as  
651 robust and smooth kinematics. These stimulation protocols could be triggered by an operator at  
652 the beginning of each reach movement or automatically from intra-cortical signals in real-time.  
653 Therefore, we verified that movement onset could be detected from intra-cortical signals even  
654 after SCI (**Extended Data Figure 5**).  
655

656 *Stimulation during three-dimensional reach and pull task in injured monkeys*

657 All monkeys were recorded after injury as soon as they could independently move in their housing,  
658 feed themselves autonomously and did not show signs of discomfort. This corresponded to 3, 5  
659 and 6 days after injury respectively for Mk-Yg, Mk-Br and Mk-Sa. After injury, the animals were  
660 reluctant to perform the task which required intense manual activity by the trainers to encourage  
661 them with the use of special positive rewards. Moreover, in consequence of the arm and hand  
662 impairments animals were quickly exhausted. As a result, the output of consistent behavior/day  
663 was low, and we were able to collect robust data in about 1day/week per animal after SCI. Each  
664 session was organized as follows. First, we executed two blocks without stimulation, each of the  
665 duration of approximately 2 minutes. During those blocks we visually evaluated the impairment  
666 level of the animal and the performance of the brain decoder. Second, we used the brain decoder  
667 to trigger specific stimulation patterns. Contacts used to elicit those functions were defined  
668 through the experiments described in the previous paragraph and combined together to create  
669 stimulation protocols that allowed the animal to perform a full reach, grasp and pull movement.

670 *Identification and classification of arm movements for kinematic analysis*

671 We defined the movement performed by the animals as composed of three different phases:  
672 reach, grasp and pull. The identification of the reach phase was done by marking the moment in  
673 which the left hand left the metallic bar to when the hand closed around the object secured to the  
674 robot hand effector (the grasp event). The grasp phase was considered to be a window of 100  
675 ms around the moment in which hand closed around the object. The pull phase started from the  
676 grasp event and finished when the animal accomplished the task by pulling the object across the  
677 virtual spatial threshold and placed the hand back on the resting bar. Events related to the 3  
678 phases of the movement (movement onset: reaching, grasp onset: grasping and release of the  
679 object, and pulling) were identified manually by inspecting video recordings from Vicon Motion

680 Systems (Oxford, UK). The same method was applied to mark successful and complete  
681 performance of reach, grasp and pull movements as events. A successful reach was defined as  
682 a complete extension of the arm that brought the hand at the position of the target (even when  
683 grasp could not be performed). A successful grasp was defined as a successful closure of the  
684 hand around the target. A successful pull was defined as the accomplishment of a complete  
685 flexion movement that brought the target past the virtual spatial threshold. Events were then  
686 extracted from Vicon and used to perform analysis on the kinematic of the movements and to  
687 train the brain decoder by automatic routines (Matlab 2019b). All the analysis was conducted as  
688 blinded experiments.

### 689 *Decoding motor states from intracortical signals*

690 We designed a neural decoder that detected reaching and grasping events using intracortical  
691 spiking activity. In order to detect spikes, we set a threshold on each channel of -4 times the root-  
692 mean-square voltage recorded during a brief period while the monkey was at rest. We estimated  
693 firing rates in each of the motor cortical array channels by summing the multiunit spikes with a  
694 150 ms history every 0.5 ms. We used these multiunit firing rate estimates to compute a twenty-  
695 dimensional neural manifold capturing the majority of population variance<sup>62</sup>. We projected the  
696 spiking activity onto this manifold to calibrate a multiclass regularized linear discriminant analysis  
697 decoder<sup>50</sup> that predicted the labeled timing of reach and grasp events. The decoder used 500 ms  
698 of past neural activity and output the probability of observing the reach and grasp events. During  
699 calibration, we defined a probability threshold for each event ranging from 0.8 to 0.99 to optimize  
700 predictions of the timing of each event using cross-validation. Since the monkeys could not  
701 complete the task after SCI, we were unable to consistently acquire labeled training data. We  
702 therefore calibrated a decoding algorithm using reaches from a recording session of a healthy  
703 monkey. We then manually labeled attempted reaches after SCI by manual inspection of video  
704 recordings. Using canonical correlation analysis, we aligned the neural dynamics<sup>78</sup> preceding  
705 reaches on the healthy sessions to the observed neural dynamics preceding attempted reaches  
706 after SCI. These aligned dynamics were used to control the decoder trained on the healthy  
707 reaches.

708 We implemented a custom C++ software application running a control suite that used the  
709 decoding algorithm to trigger EES stimulation in real-time. The application received neural data  
710 over UDP and made predictions using the decoding algorithm at 15 ms intervals. When the output  
711 probabilities crossed the defined threshold, the application triggered preprogrammed patterns of  
712 EES.

### 713 *Analysis of muscle recruitment curves*

714 Electromyographic activity was bandpass filtered between 30 and 800 Hz with an offline 3<sup>rd</sup> order  
715 Butterworth filter and stimulus artifact were removed. For each animal, stimulation contact, muscle  
716 and stimulation amplitude, we extracted compound potentials from 50ms-long segments of  
717 electromyographic activity following a stimulation pulse. We then computed the peak-to-peak  
718 amplitude of compound potentials. Since we gave four pulses of stimulation for each selected  
719 current amplitude, we averaged across values corresponding to the same stimulation amplitude  
720 and represented as the mean recruitment value of each muscle as a function of the injected  
721 current. For each muscle, recruitment values have been subsequently normalized by the  
722 maximum value obtained for that specific muscle, provided that we obtained response saturation  
723 (and therefore maximal contraction) in at least one occasion during the session. In addition, we

724 computed a selectivity index for each muscle<sup>79</sup>.

725 In order to obtain a comprehensive measure of muscle recruitment for each contact that would  
726 allow to compare across animals, we computed, for each animal, each muscle and each contact,  
727 an Average Recruitment Index (ARI) as the average of the recruitment values across all  
728 stimulation amplitudes used from a specific stimulation site.

729 To compute muscle recruitment during the delivery of pulse train stimulation, we computed the  
730 energy of the EMG signal during the duration of stimulation. We then applied the same  
731 normalization procedure described above for single pulse recruitment.

### 732 Analysis of muscle activity during EES

733 Electromyographic activity was bandpass filtered between 30 and 800 Hz with an offline 3<sup>rd</sup> order  
734 Butterworth filter and stimulus artifact were removed. In all animals we computed the energy EMG  
735 signals, for each implanted muscle. Energy of EMG signals during stimulation was computed on  
736 each segment in which stimulation was delivered after the animal started a movement attempt,  
737 with the formula here below:

$$738 \quad EN_{EMG} = \frac{1}{N} \sum_i^N \|EMG_i\|^2 dt$$

739 Where  $EMG_i$  is the value of EMG activity at sample  $i$ ,  $N$  is the number of samples in the signal  
740 and  $dt$  is the sampling resolution.

741 Energy of EMG signals without stimulation was computed on each segment in which stimulation  
742 was not delivered and the animal started a movement attempt. A movement attempt was defined  
743 as an increased EMG activity of the Biceps and Deltoid muscles.

744

### 745 Analysis of task performance

746 We computed task performance with two different measures. First, we computed the success rate  
747 as the percentage of successful movement across all movement attempts. Successful  
748 movements were identified by a blind experimenter as movements performed skillfully and until  
749 the end (see above, *Identification and classification of arm movements for kinematic analysis*).  
750 Movement attempts were identified as all movements executed in response to a *go* cue and  
751 included successful movements too. Second, we computed the task performance frequency as  
752 the rate of successful movements per unit of time. In order to do this, we subdivided sessions in  
753 time bins of 2 seconds and we marked the presence or absence of successful trials, both with  
754 and without stimulation. We then used bootstrap to analyze significance of those results. We  
755 normalized all the results by the mean success rate during stimulation.

### 756 Analysis of kinematics performance

757 We performed Principal Component Analysis on a large set of kinematic features. We computed  
758 the features on data segments during the reach phase and the pull phase (see movement  
759 identification explained above, section *Identification and classification of arm movements for*  
760 *kinematic analysis*). All kinematic signals were previously low pass filtered at 6 Hz. Segments

761 were not interpolated nor resampled. Before performing PCA analysis, features were centered to  
762 have mean 0 and scaled to have standard deviation of 1 (Matlab 2019). The computed features  
763 for Mk-Br included: minimum value, maximum value and total excursion of joint angles (shoulder  
764 flexion, elbow flexion, and wrist pronation); maximum, minimum and average angular velocity (for  
765 the shoulder flexion, elbow flexion and wrist pronation); minimum, maximum and average position  
766 along the sagittal, frontal and vertical axis of each arm joint (shoulder, elbow, wrist); maximum  
767 minimum and average wrist velocity along the sagittal, frontal and vertical axis; movement  
768 smoothness<sup>77</sup>; trajectory length during and time required to complete movements. All the listed  
769 features have been computed identically during the reach phase and the pull phase separately  
770 and treated as different features. In addition, computed maximal applied three-dimensional pulling  
771 force and the average position along the sagittal, frontal and vertical axis of each arm joint  
772 (shoulder, elbow, wrist) during grasp.

773 Since for Mk-Yg we only extracted 2D kinematics on the sagittal plane, the kinematic features for  
774 Mk-Yg included: minimum value, maximum value and total excursion of joint angles (shoulder  
775 flexion and elbow flexion); maximum and average angular velocity (for the shoulder flexion and  
776 elbow flexion); minimum, maximum and average position along the sagittal and vertical axis of  
777 each arm joint (shoulder, elbow, wrist); maximum and average wrist velocity along the sagittal  
778 and vertical axis; movement smoothness<sup>77</sup>; trajectory length during and time required to complete  
779 movements. All the listed features have been computed during the reach phase.

#### 780 Processing of cortical signals

781 We identified spiking events on each channel when the band-pass filtered signal (250 Hz–5kHz)  
782 exceeded 3.0–3.5 times its root-mean-square value calculated over a period of 5s. We removed  
783 artifacts by deleting all the spikes that synchronously in at least 30 channels. We computed the  
784 firing rate of each channel as the number of spikes detected over non-overlapping bins of 10ms.  
785 Whenever we showed average firing rate activity, we sorted channels in order of activation in one  
786 reference trial, and subsequently applied the same ordering method to all other trials. Finally, we  
787 normalized the activity of each channel by its maximum firing rate.

#### 788 Comparison of motor cortical activity during EES evoking movement and no movement

789 To study how motor cortical activity interacted with EES, we analyzed the neural recordings from  
790 Mk-Br and Mk-Yg. We identified periods where EES pulse trains produced no discernible  
791 movements by setting a threshold on hand velocity. We compared multi-unit neural firing rates on  
792 each channel in this period to neural firing rates in the previously identified trials where EES  
793 enabled reaching and grasping. First, we counted the number of spikes within the window of  
794 stimulation and divided by the duration of stimulation. We then averaged across stimulus  
795 repetitions of the movement and no movement conditions and pooled across recording sites in  
796 motor cortex.

797 We next computed instantaneous estimates of multi-unit firing rates on each channel by counting  
798 the number of spikes in non-overlapping 20 ms bins and convolving with a gaussian kernel of 50  
799 ms width. We applied Principal Component Analysis (PCA) to compute 10-dimensional neural  
800 manifolds spanning this multi-unit population activity<sup>62</sup>. We projected the neural activity onto these  
801 manifold axes during the periods where EES evoked either movement or no movement. We then  
802 identified periods where the monkey was at rest with no EES, as well as periods where the  
803 monkey attempted movements of the arm with no EES. To compare the similarity of neural activity

804 between these conditions, we computed the Mahalanobis distance between activity at rest and  
805 the three other periods: EES with movement, EES with no movement, and attempted movements  
806 with no EES.

### 807 Histology

808 Monkeys were deeply anesthetized (lethal dose of pentobarbital, 60mg/kg, injected i.v.) and  
809 transcardially perfused with saline (about 200 ml), followed by 3 liters of 4% paraformaldehyde  
810 (PFA). Dissected spinal cord were post-fixed in 4% PFA overnight, and then immersed in 30%  
811 sucrose solution for 2 weeks. 50 $\mu$ m transverse or horizontal sections were cut using a cryostat  
812 and kept in 0.1M PBS azide (0.03%) at 4°C. Primary antibodies were: rabbit anti-Iba1 (1:1000,  
813 Wako) and guinea pig anti-NeuN (1:300, Millipore). Fluorescence secondary antibodies were  
814 conjugated to: Alexa fluor 647 and Alexa fluor 555 (Life technologies). Sections were coverslipped  
815 using Mowiol. Immunofluorescence was imaged digitally using a slide scanner (Olympus VS-120).  
816 Lesions were reconstructed using image analysis software (NeuroLucida) to trace the lesion over  
817 serial sections (200  $\mu$ m apart).

### 818 Statistical procedures

819 All data are reported as mean values  $\pm$  standard error of the mean (s.e.m.) or mean values  $\pm$   
820 standard deviation (std). The choice is highlighted directly in the figures or in the relative caption.  
821 Significance was analyzed using the non-parametric Wilcoxon rank-sum test. In the comparisons  
822 shown in Figure 3 we subsequently applied the Bonferroni correction. In only one case (Figure  
823 4A, 4B, 4C), significance was analyzed using bootstrap. The level of significance was set at  
824 \* $p < 0.05$ , \*\* $p < 0.01$ , \*\*\* $p < 0.001$ .

825



826

827 **References**

828

829

1. ICCP. International Campaign for Cures of Spinal Cord Injury Paralysis.

830

<http://www.campaignforcure.org>.

831

2. National Center for Chronic Disease Prevention and Health Promotion , Division for Heart

832

Disease and Stroke. Stroke Facts. <https://www.cdc.gov/stroke/facts.htm> (2020).

833

3. Anderson, K. D. Targeting recovery: priorities of the spinal cord-injured population. *Journal*

834

*of neurotrauma* **21**, 1371–1383 (2004).

835

4. Moreland, J. D. *et al.* Needs assessment of individuals with stroke after discharge from

836

hospital stratified by acute Functional Independence Measure score. *Disability and*

837

*rehabilitation* **31**, 2185–2195 (2009).

838

5. Lemon, R. N. Descending pathways in motor control. *Annual review of neuroscience* **31**,

839

195–218 (2008).

840

6. Griffin, D. M., Hoffman, D. S. & Strick, P. L. Corticomotoneuronal cells are ‘functionally

841

tuned’. *Science* **350**, 667–70 (2015).

842

7. Griffin, D. M. & Strick, P. L. The motor cortex uses active suppression to sculpt movement.

843

*Sci Adv* **6**, eabb8395 (2020).

844

8. Seki, K., Perlmuter, S. I. & Fetz, E. E. Sensory input to primate spinal cord is

845

presynaptically inhibited during voluntary movement. *Nat Neurosci* **6**, 1309–16 (2003).

846

9. Lebedev, M. A. & Nicolelis, M. A. Brain-machine interfaces: From basic science to

847

neuroprostheses and neurorehabilitation. *Physiological reviews* (2017).

848

10. Ethier, C., Oby, E. R., Bauman, M. J. & Miller, L. E. Restoration of grasp following paralysis

849

through brain-controlled stimulation of muscles. *Nature* **485**, 368–371 (2012).

850

11. Moritz, C. T., Perlmuter, S. I. & Fetz, E. E. Direct control of paralysed muscles by cortical

851

neurons. *Nature* **456**, 639–642 (2008).

- 852 12. Bouton, C. E. *et al.* Restoring cortical control of functional movement in a human with  
853 quadriplegia. *Nature* (2016) doi:10.1038/nature17435.
- 854 13. Ajiboye, A. B. *et al.* Restoration of reaching and grasping movements through brain-  
855 controlled muscle stimulation in a person with tetraplegia: a proof-of-concept demonstration.  
856 *The Lancet* (2017) doi:10.1016/S0140-6736(17)30601-3.
- 857 14. Giat, Y., Mizrahi, J. & Levy, M. A musculotendon model of the fatigue profiles of paralyzed  
858 quadriceps muscle under FES. *IEEE transactions on biomedical engineering* **40**, 664–674  
859 (1993).
- 860 15. Popovic, M. R., Popovic, D. B. & Keller, T. Neuroprostheses for grasping. *Neurological*  
861 *research* **24**, 443–452 (2002).
- 862 16. Edgerton, V. R. *et al.* Training locomotor networks. *Brain Res Rev* **57**, 241–254 (2008).
- 863 17. Holinski, B. J. *et al.* Intraspinal microstimulation produces over-ground walking in  
864 anesthetized cats. *J Neural Eng* **13**, 056016 (2016).
- 865 18. Zimmermann, J. B., Seki, K. & Jackson, A. Reanimating the arm and hand with intraspinal  
866 microstimulation. *Journal of neural engineering* **8**, 054001 (2011).
- 867 19. Gaunt, R. A., Prochazka, A., Mushahwar, V. K., Guevremont, L. & Ellaway, P. H. Intraspinal  
868 microstimulation excites multisegmental sensory afferents at lower stimulus levels than local  
869  $\alpha$ -motoneuron responses. *Journal of neurophysiology* **96**, 2995–3005 (2006).
- 870 20. Rattay, F., Minassian, K. & Dimitrijevic, M. R. Epidural electrical stimulation of posterior  
871 structures of the human lumbosacral cord: 2. quantitative analysis by computer modeling.  
872 *Spinal cord* **38**, 473–489 (2000).
- 873 21. Capogrosso, M. *et al.* A computational model for epidural electrical stimulation of spinal  
874 sensorimotor circuits. *The Journal of neuroscience : the official journal of the Society for*  
875 *Neuroscience* **33**, 19326–40 (2013).

- 876 22. Moraud, E. M. *et al.* Mechanisms Underlying the Neuromodulation of Spinal Circuits for  
877 Correcting Gait and Balance Deficits after Spinal Cord Injury. *Neuron* **89**, 814–28 (2016).
- 878 23. Formento, E. *et al.* Electrical spinal cord stimulation must preserve proprioception to enable  
879 locomotion in humans with spinal cord injury. *Nature neuroscience* **21**, 1728 (2018).
- 880 24. Wenger, N. *et al.* Closed-loop neuromodulation of spinal sensorimotor circuits controls  
881 refined locomotion after complete spinal cord injury. *Science translational medicine* **6**,  
882 255ra133-255ra133 (2014).
- 883 25. Harkema, S. *et al.* Effect of epidural stimulation of the lumbosacral spinal cord on voluntary  
884 movement, standing, and assisted stepping after motor complete paraplegia: a case study.  
885 *The Lancet* **377**, 1938–1947 (2011).
- 886 26. Angeli, C. A., Edgerton, V. R., Gerasimenko, Y. P. & Harkema, S. J. Altering spinal cord  
887 excitability enables voluntary movements after chronic complete paralysis in humans. *Brain*  
888 **137**, 1394–1409 (2014).
- 889 27. Ichiyama, R. M., Gerasimenko, Y. P., Zhong, H., Roy, R. R. & Edgerton, V. R. Hindlimb  
890 stepping movements in complete spinal rats induced by epidural spinal cord stimulation.  
891 *Neurosci Lett* **383**, 339–44 (2005).
- 892 28. Courtine, G. *et al.* Transformation of nonfunctional spinal circuits into functional states after  
893 the loss of brain input. *Nat Neurosci* **12**, 1333–1342 (2009).
- 894 29. van den Brand, R. *et al.* Restoring Voluntary Control of Locomotion after Paralyzing Spinal  
895 Cord Injury. *Science* **336**, 1182–1185 (2012).
- 896 30. Harkema, S. *et al.* Effect of epidural stimulation of the lumbosacral spinal cord on voluntary  
897 movement, standing, and assisted stepping after motor complete paraplegia: a case study.  
898 *Lancet* **377**, 1938–47 (2011).
- 899 31. Grahn, P. J. *et al.* Enabling Task-Specific Volitional Motor Functions via Spinal Cord  
900 Neuromodulation in a Human With Paraplegia. *Mayo Clin Proc* **92**, 544–554 (2017).

- 901 32. Angeli, C. A. *et al.* Recovery of Over-Ground Walking after Chronic Motor Complete Spinal  
902 Cord Injury. *N Engl J Med* **379**, 1244–1250 (2018).
- 903 33. Gill, M. L. *et al.* Neuromodulation of lumbosacral spinal networks enables independent  
904 stepping after complete paraplegia. *Nat Med* (2018) doi:10.1038/s41591-018-0175-7.
- 905 34. Alam, M. *et al.* Evaluation of optimal electrode configurations for epidural spinal cord  
906 stimulation in cervical spinal cord injured rats. *Journal of neuroscience methods* **247**, 50–57  
907 (2015).
- 908 35. Lu, D. C. *et al.* Engaging Cervical Spinal Cord Networks to Reenable Volitional Control of  
909 Hand Function in Tetraplegic Patients. *Neurorehabil Neural Repair* **30**, 951–962 (2016).
- 910 36. Inanici, F., Brighton, L. N., Samejima, S., Hofstetter, C. P. & Moritz, C. T. Transcutaneous  
911 spinal cord stimulation restores hand and arm function after spinal cord injury. *IEEE Trans*  
912 *Neural Syst Rehabil Eng* Online ahead of print-Online ahead of print (2021)  
913 doi:10.1109/TNSRE.2021.3049133.
- 914 37. Kapadia, N., Zivanovic, V. & Popovic, M. Restoring voluntary grasping function in individuals  
915 with incomplete chronic spinal cord injury: pilot study. *Topics in spinal cord injury*  
916 *rehabilitation* **19**, 279–287 (2013).
- 917 38. Grillner, S. The motor infrastructure: from ion channels to neuronal networks. *Nat Rev*  
918 *Neurosci* **4**, 573–586 (2003).
- 919 39. McCrea, D. A. & Rybak, I. A. Organization of mammalian locomotor rhythm and pattern  
920 generation. *Brain Res Rev* **57**, 134–46 (2008).
- 921 40. Bizzi, E., Giszter, S. F., Loeb, E., Mussa-Ivaldi, F. A. & Saltiel, P. Modular organization of  
922 motor behavior in the frog's spinal cord. *Trends in neurosciences* **18**, 442–446 (1995).
- 923 41. Giszter, S. F. Motor primitives--new data and future questions. *Curr Opin Neurobiol* **33**,  
924 156–65 (2015).

- 925 42. Alstermark, B. & Isa, T. Circuits for skilled reaching and grasping. *Annu Rev Neurosci* **35**,  
926 559–78 (2012).
- 927 43. Lemon, R. N. & Griffiths, J. Comparing the function of the corticospinal system in different  
928 species: organizational differences for motor specialization? *Muscle & Nerve: Official*  
929 *Journal of the American Association of Electrodiagnostic Medicine* **32**, 261–279 (2005).
- 930 44. Kinoshita, M. *et al.* Genetic dissection of the circuit for hand dexterity in primates. *Nature*  
931 **487**, 235–238 (2012).
- 932 45. Weiler, J., Gribble, P. L. & Pruszynski, J. A. Spinal stretch reflexes support efficient hand  
933 control. *Nat. Neurosci* 1–11 (2019).
- 934 46. Omrani, M., Murnaghan, C. D., Pruszynski, J. A. & Scott, S. H. Distributed task-specific  
935 processing of somatosensory feedback for voluntary motor control. *Elife* **5**, e13141 (2016).
- 936 47. Sauerbrei, B. A. *et al.* Cortical pattern generation during dexterous movement is input-  
937 driven. *Nature* **577**, 386–391 (2020).
- 938 48. Wenger, N. M. M., E; Gandar, J; Musienko, P; Capogrosso, M; Baud, L; Legoff, C; Barraud,  
939 Q; Pavlova, N; Domonici N; Minev, I; Asboth, L; Hirsch, A; Duis, S; Kreider, J; Mortera, A;  
940 Haverbeck, O; Kraus, S; Schmitz, F; DiGiovanna, J; van den Brand, R; Bloch, J; Detemple,  
941 P; Lacour, S; Bezard, E; Micera, S; Courtine G. Spatiotemporal neuromodulation therapies  
942 engaging muscle synergies to improve motor control after spinal cord injury. *Nature*  
943 *Medicine* (2015).
- 944 49. Capogrosso, M. *et al.* Configuration of electrical spinal cord stimulation through real-time  
945 processing of gait kinematics. *Nat Protoc* (2018) doi:10.1038/s41596-018-0030-9.
- 946 50. Capogrosso, M. *et al.* A brain–spine interface alleviating gait deficits after spinal cord injury  
947 in primates. *Nature* **539**, 284–288 (2016).
- 948 51. Wagner, F. B. *et al.* Targeted neurotechnology restores walking in humans with spinal cord  
949 injury. *Nature* **563**, 65 (2018).

- 950 52. Ladenbauer, J., Minassian, K., Hofstoetter, U. S., Dimitrijevic, M. R. & Rattay, F. Stimulation  
951 of the Human Lumbar Spinal Cord With Implanted and Surface Electrodes: A Computer  
952 Simulation Study. *Neural Systems and Rehabilitation Engineering, IEEE Transactions on*  
953 **18**, 637–645 (2010).
- 954 53. Greiner, N. *et al.* Recruitment of Upper-Limb Motoneurons with Epidural Electrical  
955 Stimulation of the Primate Cervical Spinal Cord. *Nat Commun* (2021).
- 956 54. Barra, B. *et al.* A Versatile Robotic Platform for the Design of Natural, Three-Dimensional  
957 Reaching and Grasping Tasks in Monkeys. *Journal of Neural Engineering* (2019)  
958 doi:10.1088/1741-2552/ab4c77.
- 959 55. Jenny, A. B. & Inukai, J. Principles of motor organization of the monkey cervical spinal cord.  
960 *J Neurosci* **3**, 567–75 (1983).
- 961 56. Capogrosso, M. *et al.* A brain-spine interface alleviating gait deficits after spinal cord injury  
962 in primates. *Nature* **539**, 284–288 (2016).
- 963 57. Schiavone, G. *et al.* Soft, Implantable Bioelectronic Interfaces for Translational Research.  
964 *Advanced Materials* **32**, 1906512 (2020).
- 965 58. Chao, Z. C., Sawada, M., Isa, T. & Nishimura, Y. Dynamic Reorganization of Motor  
966 Networks During Recovery from Partial Spinal Cord Injury in Monkeys. *Cereb Cortex* (2018)  
967 doi:10.1093/cercor/bhy172.
- 968 59. Freund, P. *et al.* Nogo-A–specific antibody treatment enhances sprouting and functional  
969 recovery after cervical lesion in adult primates. *Nature medicine* **12**, 790–792 (2006).
- 970 60. Sharpe, A. N. & Jackson, A. Upper-limb muscle responses to epidural, subdural and  
971 intraspinal stimulation of the cervical spinal cord. *J Neural Eng* **11**, 016005 (2014).
- 972 61. Gerasimenko, Y. P. *et al.* Spinal cord reflexes induced by epidural spinal cord stimulation in  
973 normal awake rats. *Journal of Neuroscience Methods* **157**, 253–263 (10).

- 974 62. Gallego, J. A., Perich, M. G., Miller, L. E. & Solla, S. A. Neural Manifolds for the Control of  
975 Movement. *Neuron* **94**, 978–984 (2017).
- 976 63. Lempka, S. F. *et al.* Patient-specific analysis of neural activation during spinal cord  
977 stimulation for pain. *Neuromodulation: Technology at the Neural Interface* **23**, 572–581  
978 (2020).
- 979 64. Schirmer, C. M. *et al.* Heuristic map of myotomal innervation in humans using direct  
980 intraoperative nerve root stimulation. *J Neurosurg Spine* **15**, 64–70 (2011).
- 981 65. Moritz, C. T., Lucas, T. H., Perlmutter, S. I. & Fetz, E. E. Forelimb movements and muscle  
982 responses evoked by microstimulation of cervical spinal cord in sedated monkeys. *Journal*  
983 *of neurophysiology* **97**, 110–120 (2007).
- 984 66. Kato, K., Nishihara, Y. & Nishimura, Y. Stimulus outputs induced by subdural electrodes on  
985 the cervical spinal cord in monkeys. *Journal of Neural Engineering* **17**, 016044 (2020).
- 986 67. de Freitas, R. M. *et al.* Selectivity and excitability of upper-limb muscle activation during  
987 cervical transcutaneous spinal cord stimulation in humans. *Journal of Applied Physiology*  
988 (2021).
- 989 68. Kirsch, R. & Rymer, W. Neural compensation for muscular fatigue: evidence for significant  
990 force regulation in man. *Journal of neurophysiology* **57**, 1893–1910 (1987).
- 991 69. Song, S. & Geyer, H. A neural circuitry that emphasizes spinal feedback generates diverse  
992 behaviours of human locomotion. *The Journal of physiology* (2015) doi:10.1113/JP270228.
- 993 70. Confais, J., Kim, G., Tomatsu, S., Takei, T. & Seki, K. Nerve-specific input modulation to  
994 spinal neurons during a motor task in the monkey. *Journal of Neuroscience* **37**, 2612–2626  
995 (2017).
- 996 71. Seáñez, I. & Capogrosso, M. Motor improvements enabled by spinal cord stimulation  
997 combined with physical training after spinal cord injury: review of experimental evidence in  
998 animals and humans. *Bioelectronic Medicine* **7**, 1–13 (2021).

- 999 72. Granat, M., Heller, B., Nicol, D., Baxendale, R. & Andrews, B. Improving limb flexion in FES  
1000 gait using the flexion withdrawal response for the spinal cord injured person. *Journal of*  
1001 *biomedical engineering* **15**, 51–56 (1993).
- 1002 73. Ting, J. *et al.* A wearable neural interface for detecting and decoding attempted hand  
1003 movements in a person with tetraplegia. in 1930–1933 (IEEE, 2019).
- 1004 74. National Research Council (US) Institute for Laboratory Animal Research. *Guide for the*  
1005 *Care and Use of Laboratory Animals*. (National Academies Press (US), 1996).
- 1006 75. Mathis, A. *et al.* DeepLabCut: markerless pose estimation of user-defined body parts with  
1007 deep learning. *Nature neuroscience* **21**, 1281–1289 (2018).
- 1008 76. Toossi, A. *et al.* Effect of anesthesia on motor responses evoked by spinal neural  
1009 prostheses during intraoperative procedures. *Journal of neural engineering* **16**, 036003  
1010 (2019).
- 1011 77. Teulings, H.-L., Contreras-Vidal, J. L., Stelmach, G. E. & Adler, C. H. Parkinsonism  
1012 Reduces Coordination of Fingers, Wrist, and Arm in Fine Motor Control. *Experimental*  
1013 *Neurology* **146**, 159–170 (1997).
- 1014 78. Gallego, J. A., Perich, M. G., Chowdhury, R. H., Solla, S. A. & Miller, L. E. Long-term  
1015 stability of cortical population dynamics underlying consistent behavior. *Nature*  
1016 *neuroscience* **23**, 260–270 (2020).
- 1017 79. Raspopovic, S., Capogrosso, M. & Micera, S. A Computational Model for the Stimulation of  
1018 Rat Sciatic Nerve Using a Transverse Intrafascicular Multichannel Electrode. *IEEE*  
1019 *Transactions on Neural Systems and Rehabilitation Engineering* **19**, 333–344 (2011).  
1020